Virtual Inertia Emulation

in islanded microgrids with energy storage system

Yuguang Zheng

Technische Universiteit Delft

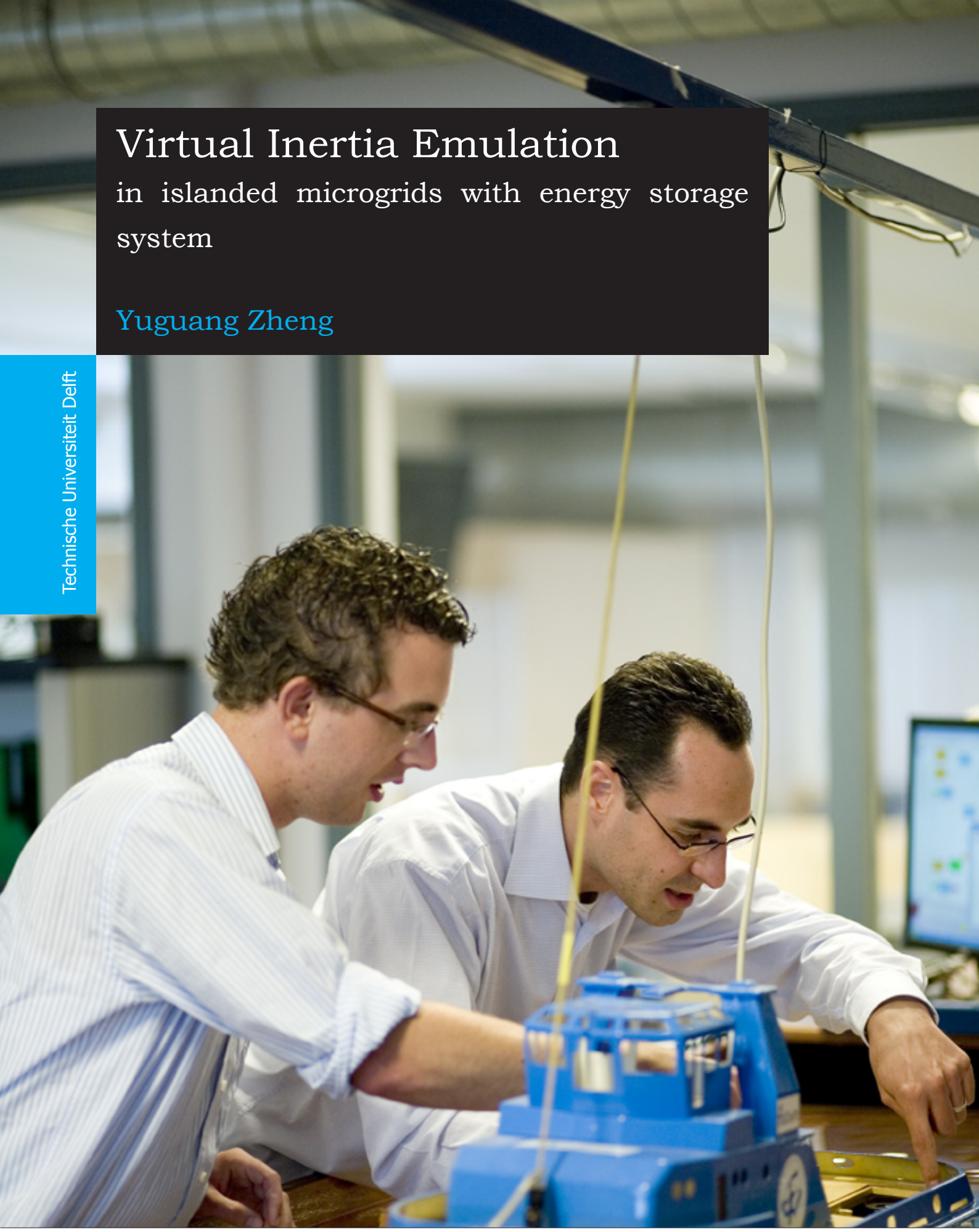

TU Delft Delft University of Technology

Challenge the future

Virtual Inertia Emulation

in islanded microgrids with energy storage system

by

Yuguang Zheng

in partial fulfillment of the requirements for the degree of

Master of Science
in Electrical Engineering, Mathematics and Computer Science

at the Delft University of Technology,
to be defended publicly on Tuesday August 30, 2016 at 1:00 PM.

Supervisor:	Dr. L. R. Elizondo	
Thesis committee:	Prof. dr. Pavol Bauer,	TU Delft
	Dr. L. R. Elizondo,	TU Delft
	Dr. Milos Cvetkovic,	TU Delft

TU Delft Delft University of Technology

Summary

The inertial response plays a vital role in electrical networks to reduce the rate of change of frequency (RoCoF) following a contingency event. If the inertia has a low or zero value due to a lack of synchronous generators, then the electrical network might experience large undesirable frequency deviations. To overcome this problem, in previous research, mathematical methods have been emerged to enhance the system stability in current source based microgrids. The battery energy storage system embodies the isolated microgrid operates as voltage source and the implementation of the demand side management in which frequency is used as a communication signal. The requirement for inertia frequency response is indicated. In this work, the power electronics methods to emulate virtual inertia have been found, developed and compared.

An overview of existing methods has been presented, which includes the introduction of the principles and comparison between their advantages and disadvantages. Based on those techniques, an additional PID controller has been recommended for the isolated microgrids working as current source. Furthermore, three control schemes to incite inertial responses have been developed for the microgrids in voltage source type as follows: 1) swing equation method, 2) low pass filter, and 3) an adjustable rate limiter. introducing swing equation, adding low-pass filter and setting rate limiter.

Case studies to test and compare the proposed methods have been established. Accordingly, the corresponding dynamic models of investigated microgrids are created by Simulink graphical blocks. The models allow the study of the voltage source based islanded network in similar conditions as the current source based system, and facilitates their comparison. Therefore, the project includes the comparison between the system behaviors with and without additional inertia control loops in islanded networks with and without rotating mass synchronous generators, respectively. The different responses in the two source types also have been discussed.

Inverter dominates the system frequency in microgrid based on voltage source. Compare to the frequency managed by original droop control, the implemented control schemes slow down its changing speed and the system inertial level can be manipulated by adjusting coefficients. Their performance characteristics correspond to the involved extra functions. The PID control in current source - diesel system supports the energy supply and reduces frequency deviation. The proportional equation and the differential equation affect the grid in different ways. Unlike the ideal power reaction in voltage source system, the performance of the current source based islanded microgrid are more improvable and uncontrollable.

Acknowledgements

It has been two years since my first day in Delft. I learn a lot in the two-year master study program and the nine month of thesis research. I would like to extend my gratitude to Laura Ramirez Elizondo and Seyemahdi Izadkhast for their guidance, comments and support throughout this project. I would also like to thank my parents for their support throughout my studies.

Yuguang Zheng
Delft, August 2016

Contents

Nomenclature

$BESS$ battery energy storage system

CC current control

$CSGriP$ Cellular Smart Grid Platform

DG distributed generator

ESS energy storage system

LP Low-pass

MG microgrid

$MPPT$ Maximum Power Point Track

$P-f$ active power - frequency

$PHDET$ phase detector

PID proportional, integral, and derivative

PQ active power reactive power

RES renewable energy source

RL rate limiter

$RoCoF$ rate of change of frequency

SoC state of charge

$SOPRA$ Sustainable Off-grid Power plant for Rural Applications

VC voltage control

VSG virtual synchronous generator

List of Figures

List of Tables

1

Introduction,Context,Contributions

1.1. Introduction

Due to the increasing energy demand and intensive oil crisis in the world, renewable energies have played a significant role in power consumption, especially in electricity generation. In recent years, the capacity of the installed distributed generators (DGs) in power system grows rapidly. Significant targets are also considered for using the DGs and Renewable Energy Sources (RESs) in their power systems up to next two decades in European countries, USA, China, and India.

Stability in a power system refers to the capability of an electric power grid to recover to an operating equilibrium after undergoing a disturbance or operating state change, with most parts of the network remaining intact [1]. In traditional power systems, the synchronous generators driven by primary source (mainly from coal) and the rotor-frequency characteristic (inertia property) stabilize the network's performance. Compared to the conventional bulk power plants, the DGs have either very low or no inertia level which could lead to severe impacts in the system which could be:

- A low level of stability or even frequency instability.
- High amplitude frequency oscillations
- High rate of change of frequency (RoCoF)
- Devices tripped offline

As a fact of converter connected distributed generation units extending their integration capacity in the whole system, the system stability has become a critical issue. This thesis works

on the methods to enhance the reliability of isolated microgrids (MGs) by providing additional virtual inertia.

1.2. SOPRA and Csgrip project

The Sustainable Off-grid Power plant for Rural Applications (SOPRA™) is a system developed by Alfen, which aims at electrifying rural areas using RESs sources. SOPRA is a container-based setup which consists of inverters, battery banks, a advanced control system and smart meters on the consumer end that carry out demand side management procedures. Cellular Smart Grid Platform (CSGriP™) is a successor of Csgrip is aiming to form larger, stronger and more robust islanded grids, using mainly sustainable energy sources. Because of the variation of power output by the uncontrollable RESs, energy storage system (ESS) is used as a long-term storage device and deals with the mismatch between the generated power and load demand in this project.

This thesis supports the researches in CSGriP project and it will mainly focus on the different control schemes as solutions towards stabilizing the RESs based MGs by emulating additional virtual inertia via power electronics. It's necessary to propose appropriate solutions for the different operation states of MGs in CSGriP project. This approach will contribute to the stability and reliability of the MGs. Furthermore, it may provide some ideas for maintaining a large share of RESs without compromising system security.

1.3. Motivations

Inertia in power system slows down the decline (or rise) of frequency when a sudden change takes place in the generation units or in the electricity demand. The inertial characteristic in power system helps prevent protective load shedding mechanisms from kicking in by providing time for compensating control systems to adjust generation to the changing environment. Lack of inertia in power system could cause power grid instability. As the RESs-based distributed generation units begin to increase their footprint on the electric networks, inertia in microgrid has become a topic of more interest. In general, the two main sources of inertia in the power system are the classic synchronous generators (typically steam turbines) and the large industrial motors. On the other hand, the renewable resources, which could be the PV cells, being connected from the generation units to the grid through the power electronic inverters which could not provide any inertia to the system. Therefore, in the MGs without connection to the main grid, there is either very slight or no inertia property, which could lead to the severe impacts to the microgrid system as mentioned in the first section.

In the islanded MGs in Csgrip project, the most typical operation mode is the voltage-source mode. In this circumstance, the battery energy storage system (BESS) becomes the only power supply, and replying on a communication signal the electricity devices are managed.

However, the RESs are intermittent, and the generation could be the affected by location of generation units, the local weather. The further step is to connect the MGs to other sources such as diesel and the main grid. In this case, the BESS works as a current source and transmit a specific amount of power into the grid. Inertia emulation methods should be proposed/developed and compared to intensify the system stability in both of the scenarios.

1.4. Objectives and Research questions

1.4.1. Main Objectives

Propose and develop methods to emulate virtual inertia for the islanded microgrids including BESS via power electronics.

1.4.2. Specific Objectives

1. Develop or propose appropriate electronic control schemes for providing additional virtual inertia for battery based islanded microgrids (means for the voltage source and current source, respectively);
2. Study and develop the inverter control loops and model the islanded system where the battery works as a voltage source. Implement droop control in the MG system and set appropriate droop control coefficient.
3. Enable the additional control scheme(s), which enhances the frequency inertial performance, in a microgrid with and without a diesel.
4. Review existing methods for virtual inertia emulation. Discuss their operation scopes and limitations.

1.4.3. Research questions

1. Distributed generation units based Microgrids operate in various modes and situations. The network is quite stable in some of the conditions, and additional control methods to provide virtual inertia is required in some other states. What are the characteristics of the MGs running modes and what are the impacts of low inertia property?
2. Researches on inertia emulation in MGs have been done in recent years. What are the existing methods to virtual inertia emulation in islanded MGs and their service scopes (limitations)?
3. The principle of a current source is not the same with a voltage source. The controllers for voltage-source based MGs and current-source based MGs should be discussed separately. What are the additional control loops to emulate inertia for the two types of BESSs and what are the effects of the proposed schemes?

4. The proposed approaches for BESS works as voltage source and current source are tested and verified independently. What are the differences of the operation behavior of the microgrids with (voltage-source based) and without diesel ((current-source based))?

1.5. Methodology & Main contribution

To achieve the setting objectives, functions (for frequency control in inverter mechanisms) and models are proposed and developed. The proposed control approaches have been created and evaluated in the Simulink graphical block diagramming tool, within the MATLAB numerical computing integrated environment.

The main contribution of the thesis can be identified as :

- Develop the control loops to emulate virtual inertia for voltage-source unit based islanded MGs;
- Propose the control schemes to to inject inertia to microgrids including diesel engine and current source based units;
- A overview of existing methods to emulate inertia property.

1.6. Thesis Outline

$Chapter\ 2$, Background, gives background information about the behavior of rotating rotors (inertia property) in traditional power plants and classifies the operation modes of MGs. Four existing approaches of virtual inertia emulation have been introduced in $Chaper\ 3$.And then their scopes and advantages/disadvantages also have been discussed. In $Chapter\ 4$, the proposed inertia emulation control mechanism scheme for both voltage-source units based and current-source units based MGs are presented and explained, respectively. $Chapter\ 5$ describes the scenarios in case studies, and $Chapter\ 6$ gives introduction to the modeling part. The simulation results are presented and discussed in $Chapter\ 7$. At last, $Chapter\ 8$ concludes the remarks and makes recommendations for further work.

2

Background

2.1. Introduction

The operation principles in traditional centralized power systems and distributed generation units are entirely different. In transitional power plants, when there is an imbalance between the load demand and electric power supply, the rotor of the synchronous machine either speeds up or slows down to instantly rebalanced the system (the rotor increases its speed when the power supply is not enough while it decreases when the supplied power comparably exceeds). In the RES generation units, energy flows through wind turbines or PV cells connected inverters which do not provide any rotational inertia, are displacing the inertia machinery of the conventional machines efficiently. In this chapter, the inertial behavior in traditional power plants and the microgrid system are indicated as background information. Moreover, the characteristics of different operation modes of MGs and the requirement of virtual inertia are explained.

2.2. Traditional power plants

Conventional power system mainly builds on centralized power stations which transmit electrical energy via long-distance transmission lines. During the electricity generation process, a prime mover (from a turbine or an engine) is excited by the primary source, which could be fossil fuel, and drives a synchronous machine (SM), in which the mechanical power is transformed into electrical energy. In a SM, a governor controls the power output according to an operating power-frequency droop characteristic [2]. The characteristic between power and frequency droop couples output power with the rotor's rotating speed. The rotating mass provide inertia property to the system frequency and the output power of the synchronous

machine [2].

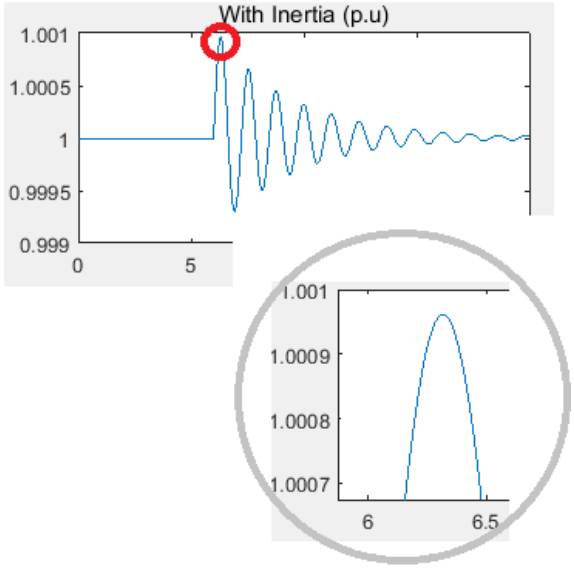

(a) Behavior with normal inertia property

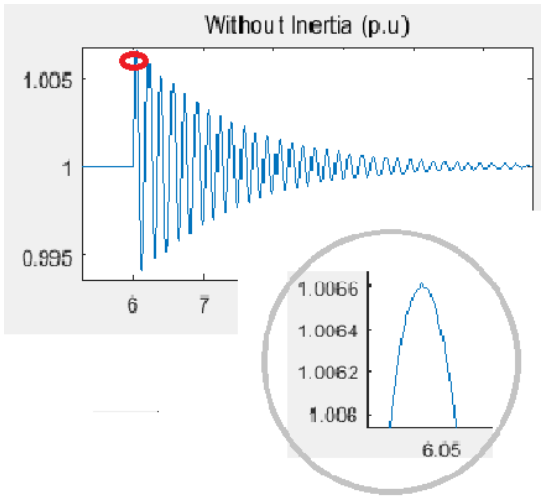

(b) Behavior with very low inertia property

Figure 2.1: Synchronous Machine behavior in traditional power plants

Numerous 7^{th} $order$ synchronous machine model has been created in MATLAB. The model simulates the behaviors of that 600MW systems with different inertia, facing 20% load change. Form the simulation results shown in Figure 2.1, rotational inertia (H) minimizes the frequency overshot and provide a slower frequency response (6 times lower overshoot and around 10 times slower changing rate). It renders frequency dynamics more benign.

2.2.1. Swing equation

The performance of a SG is influenced by the initial operating conditions and the nature of the disturbance [3]. It's central to understand the rotor's dynamic behavior to work on the electric

system stability. In [1], Equation (2.1) describes the dynamic equilibrium of the rotational behavior of a rotor. The relationship among the electromagnetic (air gap) torque ($\tau_{e,SM}(t)$), the mechanical torque ($\tau_{m,SM}(t)$) and the rotor's angle position is introduced:

$$T_{SM}\frac{\mathrm{d}^2}{\mathrm{d}t^2}\delta\theta_{SM}(t) = \tau_{m,SM}(t) - \tau_{e,SM}(t) - k_{d,SM}\frac{\mathrm{d}}{\mathrm{d}t}\delta\theta_{SM}(t) \tag{2.1}$$

where t is the time in seconds, $\delta\theta_{SM}(t)$ means the phase angle difference in electrical radians between the rotor angular position and the reference phase angle in a rotating reference frame (RRF), while $k_{d,SM}$ and T_{SM} represent the damping factor and inertia time constant, respectively [1]. T_{SM} corresponds to the time it takes rated torque to accelerate the rotor from standstill to rated speed, which is directly related to the combined moment of inertia of the SM and the prime mover. Equation (2.1) is known as the swing equation, as it describes the rotor angle swings during disturbances in power networks. The term which is proportional the to the rotor angular speed deviation(difference), is included to represent the effect of damping torque [1].

2.2.2. Rotor angle stability

In a synchronous machine based unit, the rotor's mechanical angular speed is coupled with the system frequency, therefore, the rotors of all interconnected SMs are needed to be in synchronism. The rotor angle stability refers the security level concerned with the capacity of the interconnected SMs of a power system to stay in equilibrium after undergoing a disturbance [1]. It is determined by the SMs capacity to sustain or regain equilibrium between the mechanical torque and the sum of electromagnetic torque, inertia effect and damping force [1].

When the power system experiences a disturbance or operation state change, which causes the rotors' acceleration or deceleration, and the operating equilibrium gets disrupted. If one of the SMs spins more quickly than the others, its rotor angle increases (with respect to that of the slower SMs). Driven by the active power-angle relationship, it introduces a power transfer from the slower SMs to the faster one [3]. Then the higher terms (inertia effect) in the swing equation reduces the faster rotor speed. However, due to the active power-angle relationship, an increase in the relative position (pasts a critical point) results in a decrease in the power transfer, so that the relative angle difference increases further. The rotor speed keeps oscillating until the kinetic energy from the corresponding angle deviation is subsequently absorbed by the power system [3].

2.3. Microgrids

A significant transform has been undergoing in the conventional energy structure. As mentioned in the previous section, in the traditional centralized power plant, fossil fuel is used as the primary source to drive the synchronous machines and long-distance transmission line to support the power supply system, which does damage to the environment and causes power loss during the long-distance power transmitting. Moreover, since the grid connection may be too expensive for the rural areas, numerous people live without electric. The distributed generation (DG) units based on renewable sources (RESs) such as solar, wind energy provide a solution to those problems. Microgrids, which consist a group of distributed energy sources and interconnected loads, enable local power generation for local electric burdens [4]. By extending the MGs, the transmission loss is cut down, and various sources will enhance the power system reliability and flexibility. For the place far from the main grid, islanded microgrids become the absolute choice.

2.3.1. Energy storage system in microgrids

The energy storage device, which could by electrochemical battery, becomes a crucial element in the integration of the DGs into a microgrid. As the terminal of distributed renewable sources, energy storage system not only balances the mismatch between the power generation and consumption but also plays a critical role in stabilizing the system frequency and voltage [4]. Energy is stored by ESS at the time of surplus and re-dispatched when needed. And the connected power electronic inverter in the energy storge system (ESS) fully controls the output voltage value and frequency [4].

2.3.2. Microgrids operation modes

Microgrids support a group of interconnected loads with flexible renewable sources. Compare with traditional power plants, the energy generation process in MGs is largely influenced by the local condition which could be the daily irritation, wind speed. Thus, the operation modes of MGs should be variable, and operation characteristics of the output power and frequency behavior are not the same. The microgrid operation modes is displayed in Figure 2.2, in which the source type of the RESs generation units and their operation characterises and indicated at the bottom. According to Figure 2.2, there are two operation modes of microgrids: the grid-connected mode and the stand-alone mode. Normally, a grid-connected microgrid is used to support the main grid and cover a part of the load demand. And in the stand-alone (islanded) mode, a microgrid is isolated from the main grid. In this situation, the MG's highest priority becomes to a reliable power supply to customers instead of economic benefits. The energy management strategies and system stability are different in the two modes.

When an MG is grid-connected, RES energy is transmitted from the distributed generation

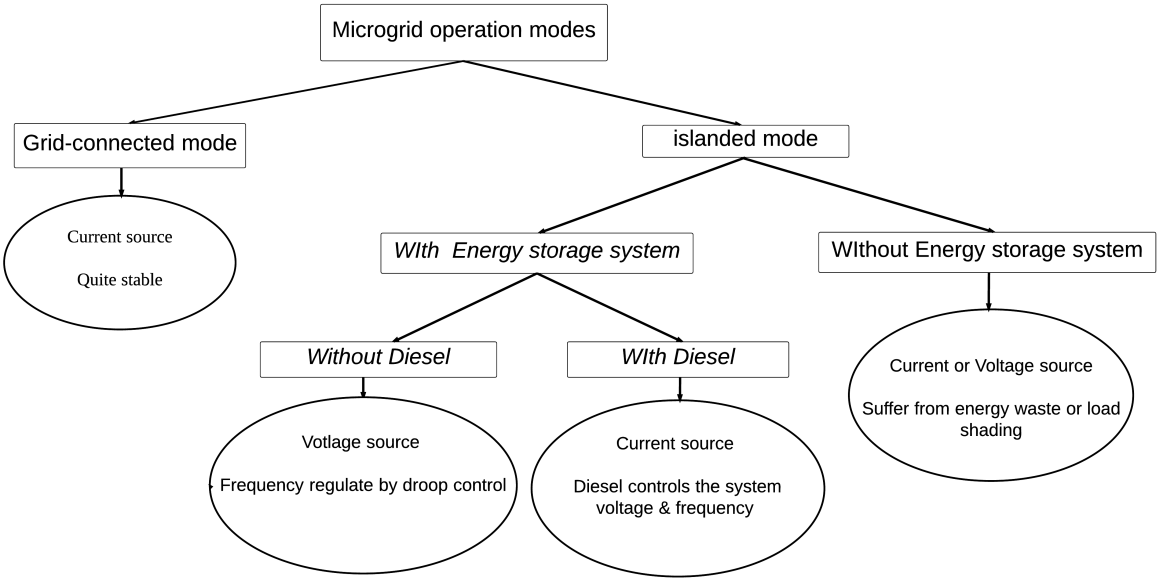

Figure 2.2: The operation modes of microgrids

units into the main grid. The system would be highly stable, e.g., the frequency deviation in Chinese central network is limited from 49.8 to 50.2, and the rate of change of frequency is extremely slow because of the rotating mass in the synchronous generators. For the grid-connected MG, the voltage value and phase angle from the MG should be synchronized with the main grid, and the MG operates in a state with strong stability for a significant amount of inertia is shared by the primary (main) network. Therefore, this thesis focuses on the microgrid working in stand-still mode.

For the stand-still microgrids, the operation modes can be distinguished by the install of battery energy storage system (BESS):

- If an islanded MG operates without an BESS, the load is restricted by the generated renewable energy, which make the system suffer continual energy waste and load shedding.
- The implement of the storage device minimizes the power, load mismatch and helps stabilize the system frequency and voltage. Regarding the islanded MGs with BESS, there are two scenarios.
  - In the first scenario, the renewable energy is abundant and able to cover all the loads in the grid. The battery turns into the only energy source in the system, and it works as a voltage source and the output power matches the load. It's noticeable that there is no device or components provide inertia in the system.
  - The second scenario refers the situation that there is not enough RES energy in an islanded MG and diesel is put to use. In this case, the battery works as a current source to cover a part of load demand, and diesel covers the rest of the electric

demand. The rotating mass in diesel provide a little inertia property the to MG system. For the current source, the sever impact of low inertial level is indicated in the first chapter.

2.3.3. Demand Side Management

load shedding and load shifting

Controlling the power consumption of the customers is used to improve the stability and reliability in voltage-source units base isolated MGs. The main techniques to implement an end-user based control are called $load\ shedding$ and $load\ shifting$ [5].

Load shedding can be applied in the conditions where the network faces over-consumption. It means a number of the operation loads are switched off, directly cutting the electricity demand. In this way, a system of stable regime can be achieved. On the other hand, load shifting is to move some of the load which occurs during the peak demand period (usually in the evening for the lightning purposes) to the moments where the power generation peaks (in case of RESs like solar: at mid-day) [5].

A precondition to apply load shedding and load shifting is to divide all the possible loads into certain groups and give them a priority level [5]. The load priority can be estimated by their importance, such as hospitals, should be in the group with highest priority. In addition, the dynamic pricing of electricity can be also considered into demand side management.

Droop speed control

Frequency is used as the communication signal of the demand side smart control and droop control is implemented in the voltage source BESS [6].

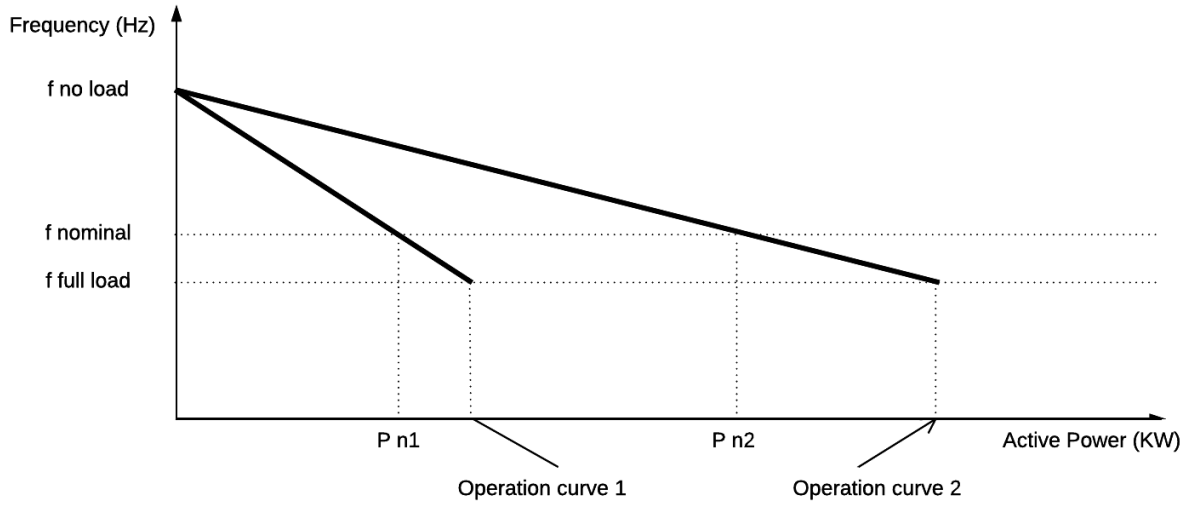

Figure 2.3: Droop speed control curves

Figure 2.3 shows the active power - frequency characteristic in droop speed control of MGs.

The droop curve is adjusted depends on the situation of the generation units. In the diagram, the operation curve 1 indicates a situation which includes low energy yield (or low battery state of charge) and the nominal power and full power is set at a basic level. When the RESs energy is plentiful, another operation curve is exploited (such as operation curve 2). By this implementation, load shedding and load shifting are applied relay on the grid frequency [6].

A significant drawback of the droop control is lack of the inertia property. When a big load is switched on or off, the frequency immediately jumped to another value. The rapidly frequency deviation may lead misoperation in the load management, and electrical equipments may be frequent switched on or off. Thence, virtual inertia is required to slow down the frequency changing speed.

2.4. Conclusion and Outlook

The rotor behavior in transitional power plants and its inertial property is explained in the second section in this chapter. Contrarily, the DG based MGs do not include the components which produce the rotating mass, and MGs operate in different modes. According to the discrepancy among the operation principle in different ways, methods for virtual inertia emulation in islanded MGs are necessary to be found, developed/proposed and compared, especially for voltage-source units based MG droop control. Existing methods should be found and studied to propose appropriate control schemes to provide additional inertia.

3

Existing methods to emulate virtual inertia

3.1. Introduction

In the previous chapter, the inertial performances in conventional power network are presented and the principles are indicated. Moreover, the structure of MGs operation modes and the requirement of power electronic methods to provide virtual inertia are explained.

Since energy consumption control in voltage-source based MG is newly proposed, targeting approaches should be developed. In [7–13], the existing methods to enhance the inertia property in current source based MGs are introduced and tested independently. [7–9, 14] gives solutions for wind farm, PV cell based islanded microgrids without ESS. [13] introduces the implication of short-term ESS to emulate inertia ability. And the concept of Virtual Synchronous Generator control, which enables BESS to mimic the dynamic behavior of a SG, is included in [10–12].

In this chapter, an overview of these methods has been posed, and their operation scopes have been discussed. Based on the discussion, the advantages and disadvantages among methods have been compared.

3.2. Virtual inertia emulation in wind farm, PV cell based islanded microgrids

As described in Figure 2.2, when an MG operates without ESS, distributed generating units such as wind farms and PV stations directly transmit RES energy to the load. The real-time generated power restricts load amount. Concerning the virtual inertia emulation, additional

control loops are set up on the converter from the generation side.

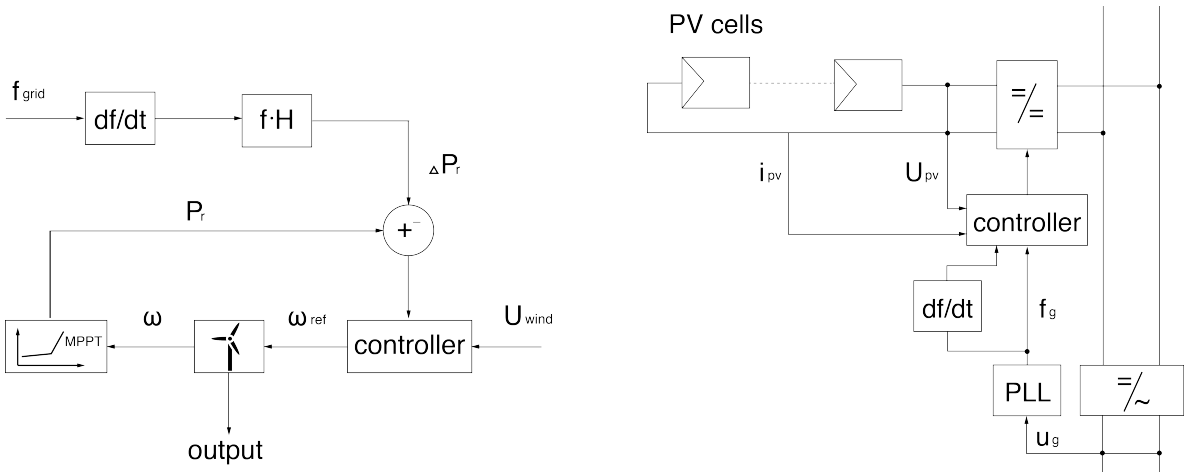

(a) Control structure for wind turbines

(b) Control structure for PV cells

Figure 3.1: Adding inertia property by wind farms and PV cells

In [7, 8, 14], cases on virtual inertia emulation for the wind turbines are offered. It's important to know that the speed of rotating rotors in wind turbines are not coupled with the system frequency, and the output power is set by power electronic converter since the wind farm operates with various wind speed. The wind farm runs as a current source, and a Maximum Power Point Track (MPPT) is practiced to manage the power generation progress. Figure 3.1(a) presents the simplified control structure. The approach is to affect the wind farm output by the cooperation MPPT with an additional control mechanism which imports a differential equation of grid frequency. Then a swing equation is introduced into the system:

$$P_{turbine} = P_{MPPT} - M_i \frac{df}{dt} \tag{3.1}$$

where M_i is the amount of interjected inertia and derivative term (it plays the role as the kinetic energy stored in the rotating rotors in synchronous machines) refers the addition energy which compensates the mismatch between grid input power and load demand.

The proposed approach in PV cells based MGs is very close to that in wind farms. In [9], extra control loops, which contain a common maximum power point tracking process, system frequency based loops, are implicated in the DC/DC converter mechanism scheme (shown in Figure 3.1(b)). The PV cells are controlled to input (or absorb) extra power when the grid frequency deviates. And the supplemental power consists the damping power (a function of Δf) and inertia power (a function of $\frac{df}{dt}$). The power supplied by PV cells is expressed by Equation (3.2).

$$p_{pv} = C_s \cdot P_{mppt} - \frac{\Delta f}{R_{pv}} - 2H_{pv}\frac{df}{dt} \tag{3.2}$$

where the C_s is a positive coefficient (smaller than 1) to ensure the approach's proper functioning (e.g. if the PV cells transmit the maximum power to the grid, there is no energy to provide inertial or damping effect when the grid frequency deviates).

Both of methods restrain the output by setting addition control scheme on the generation side converters. The system's inertia property increases with a few drawbacks. Firstly, the generation units cannot work with their maximum efficient for an amount of energy should be reserved as a guarantee. It leads to an energy waste. Worse still, the large number of extra electronic components and loops lead to a higher cost and a larger opportunity for fault taking place.

3.3. Virtual inertia emulation in MGs with diesel participation

This section addresses the problem of frequency stability in an autonomous wind-diesel power system with energy storage (at high wind penetration levels, the wind speed fluctuation causes frequency excursions which may be acceptable) and introduce the solution to the problem. In [13], an autonomous power system based on a diesel generator and a wind turbine which works in parallel is taken as an example. An energy storage (used for investigating virtual inertia) is also included, which interfaces to the ac-bus by a pulse-width modulated (PWM) converter. The converter can inject power either into two modes (the ac-bus—inverter mode or the energy storage—rectifier mode). The system operation can be characterized as Figure 3.2.

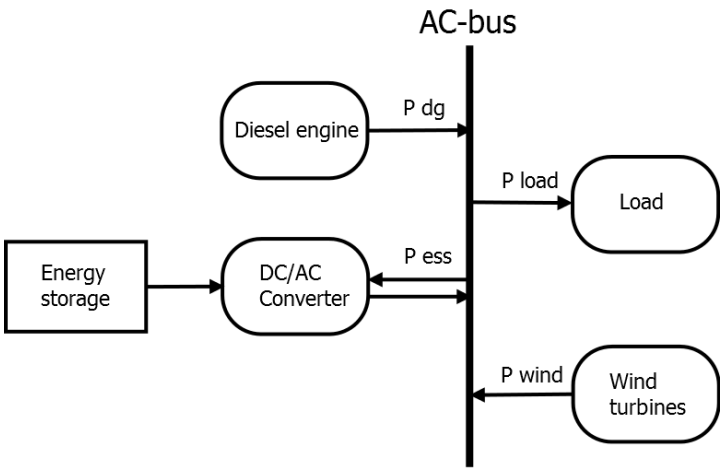

Figure 3.2: Diesel-wind system structure

The power balance in the system can be stated as:

$$P_{dg} + P_{ess} = P_{load} - P_{wg} \tag{3.3}$$

where P_{dg} is the active power of the diesel generator in service. Wind power is regarded as a negative load since both of the load and the wind energy are fluctuating resources. The ESS

power, which flows through the energy storage device and a PWM bi-directional converter, and the diesel energy are the input signals of the system.

The models for the prime mover in diesel are explained in [15–18]. The transfer function of the proposed model for the prime mover can be found. After simplifying the relationship between the fuel injection signal and rotor rotating speed, the equation of the input active power and rotor behavior is obtained.

$$J\dot{\omega}_r + k_{loss}\omega_r = \frac{p_{mech} - p_{dg}}{w_r} \tag{3.4}$$

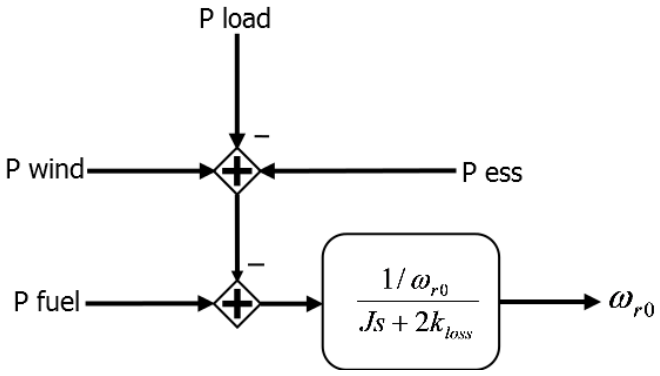

Figure 3.3: Diesel generator shaft model

In Equation (3.4), J is the inherent inertia of diesel engine, and k_{loss} is the coefficient of engine loss (caused by friction in form of heat). After replacing Equation (3.3) in Equation (3.4) and linearizing the equations, the block diagram of the diesel generator coupling shaft is obtained (Figure 3.3) [13].

Energy storage system is used to mimic the effect of the kinetic energy stored by the rotating mass of a SG. If active power through the DC/AC converter is controlled in inverse proportion to the derivative of the rotor speed, an amount if virtual inertia is emulated in the system. In this way inertial response of the diesel generator to changes in the power demand is enhanced. In this way, the inertia amount for the whole system can be regarded as the sum of inherent diesel inertia and injected inertia quantity. The formula for the DC/AC converter active power is presented by Equation (3.5).

$$p_{ess} = -k_{vi}\omega_{r0}\dot{\omega}_r \tag{3.5}$$

where $k_{vi} > 0$ is the virtual inertia gain (controls the injected inertia amount J_i). The control loop can be set after the selection of parameter k_{vi} [13]:

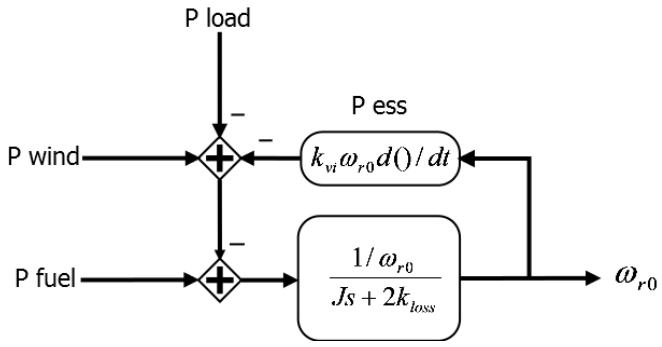

Figure 3.4: Investigate virtual inertia in diesel control

3.4. Virtual Synchronous Machine and different algorithms

Another method to emulate virtual inertia with ESS is called the Virtual Synchronous Generator (VSG) or Virtual Synchronous Machine (VISMA). It enables the DG units operating like synchronous generators, exhibiting an amount of inertia and damping properties of conventional synchronous machines for short time intervals. Then a significant share of DGs/RESs in islanded MGs can be maintained without compromising system stability by a basis from virtual inertia concept.

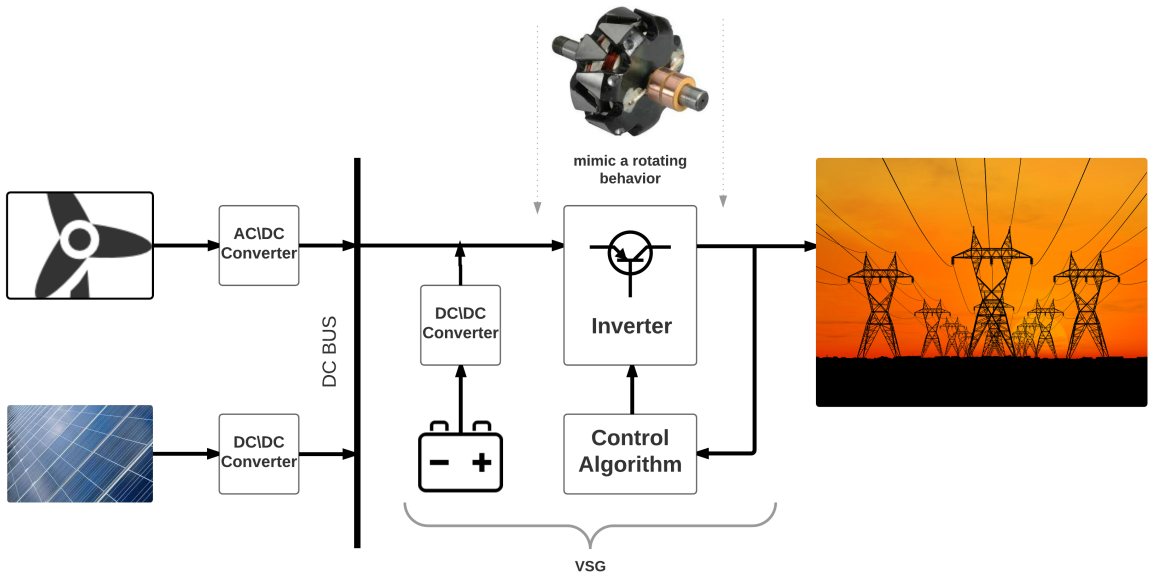

Figure 3.5: General structure and concept of the VSG

A VSG consists of energy storage, inverter, and a control mechanism as shown in Figure 3.5 [19]. And it is usually located between a DC bus and the grid. The VSG shows the DC source to the network as an SG in a viewpoint of inertia and damping property. Virtual inertia is emulated in the system by controlling the active power through the inverter in inverse proportion to the rotor speed [19]. Aside from higher frequency noise due to switching of inverter's power transistors [10], there is no difference between the electrical appearance of an electro-mechanical SG and electronics VSG, from the grid point of view.

The principle of VSG is to imitate the dynamic behavior of a SG. Equation (2.1) expresses the power-frequency characteristics in a transitional SG. From the equation, output power is described by multiplying a angle speed (ω) and the mechanic torque. Because of the angle-speed mathematics characteristics and the relationship among the terms of torque, the angular speed and the angle position. Thus the power-frequency relationship of grid with VSG unit can be described as:

$$\frac{\mathrm{d}}{\mathrm{d}t}\delta\theta_{SM}(t) = \Delta\omega = \omega - \omega_0 \tag{3.6}$$

$$\Delta P_{VSG} = P_{out} - P_{in} = K_i\frac{\mathrm{d}}{\mathrm{d}t}\Delta\omega + K_p\Delta\omega \tag{3.7}$$

where ω_0 is the nominal frequency of the grid. P_{in} indicates the transmitted power to the inverter and P_{out} is the VSG output power. The right side of Equation (3.7) means that power will be generated or absorbed by the VSG according to the initial rate of frequency change ($d\Delta\omega/dt$). And K_i expresses the inertia property of the virtual synchronous generator.

The general structure and fundamental principle of a VSG have been stated. But the algorithms in each VSG may be entirely different. There are four different algorithms (the VSYNC's, the IEPE's, the ISE Lab's and the KHI's topology). The VSYNC's topology use the Phase Locked Loops (PLL) to compute the system frequency deviation. The IEPE's topology uses a model of a synchronous machine to mimic its behavior. ISE Lab's technique sets the reference input power and measures output put power, inertia property is injected by the introduction of swing equation. And a phasor diagram and a PLL are used in the KHI's virtual generator model.

3.4.1. VSYNC's VSG topology

In [11], the structure of VYSNC(a workshop works on renewable energy in Europe) topology is shown in Figure 3.6.

A Phase Lock Loop (PLL) comprises a phase detector (PHDET), a loop filter (H) and a Voltage Controlled Oscillator (VCO). The phase detector derives a signal proportional to the frequency deviation and another signal couples to its variation rate. Depend on the Equation (3.7), the obtained two signals are used to compute the reference active power output. The preferred reactive supply is set corresponding to the voltage deviation.

$$\begin{aligned} P &= K_{SOC} + K_i\frac{df}{dt} + K_p\Delta\omega \\ Q &= K_v\Delta V \end{aligned} \tag{3.8}$$

where K_{SOC} represents the input power, which imports by the measurement of state of charge of the battery. And the reference current can be calculated by Equation (3.9) ([19]) :

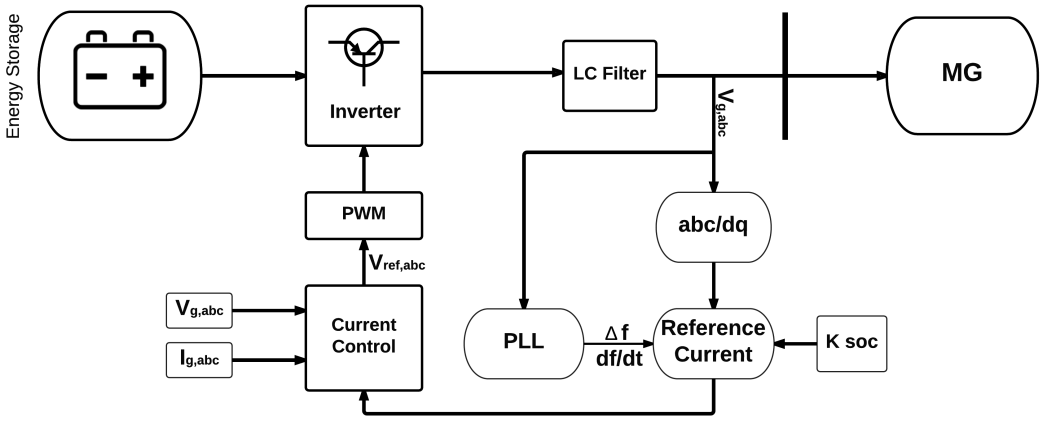

Figure 3.6: VSYNC VSG Structure

$$i_d = \frac{V_d P - V_q Q}{(V_d + V_q)^2}$$
$$i_q = \frac{V_d Q + V_q P}{(V_d + V_q)^2} \tag{3.9}$$

The reference voltage is calculated in a current controller. And the addition inertia and damping power imitate the electro-mechanical characteristic of a SG.

3.4.2. The IEPE's topology

In [10], an IEPE's (Institute of Electrical Power Eng.) VSG design, in which a simplified SG model is applied to set the reference voltage and current, is suggested. The concept is indicated in Figure 3.7 [10]. In this structure, the battery output power is controlled by adjusting the value of mechanical power (setting on the model) while the electromotive force (setting on the model) fixes the grid voltage. Moreover, the inertia quantity and damping force can be easily set and changed by adjusting the parameter of the SG model.

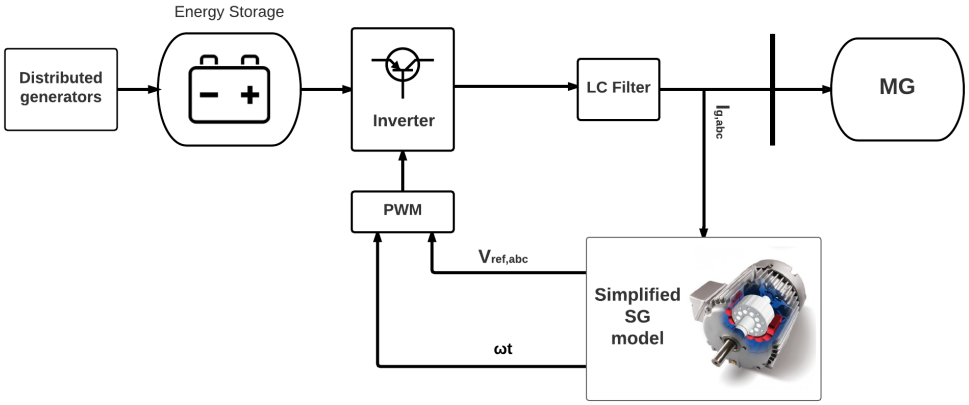

Figure 3.7: IEPE's VSG concept

The grid current ($i_{grid,abc}$) needs to be measured to compute the reference voltage value. In the SG model, the relations among the stator and rotor elements are indicated in the equations below:

Stator circuit equations:

$$\begin{aligned} e_1 - u_1 &= i_1 \cdot R_s + L_s \cdot \frac{di_1}{dt} \\ e_2 - u_2 &= i_2 \cdot R_s + L_s \cdot \frac{di_2}{dt} \\ e_3 - u_3 &= i_3 \cdot R_s + L_s \cdot \frac{di_3}{dt} \end{aligned} \tag{3.10}$$

Then represented the results by vectors:

$$\vec{e} = \begin{bmatrix} e_1 \\ e_2 \\ e_3 \end{bmatrix} \qquad \vec{i}_{gird} = \begin{bmatrix} i_1 \\ i_2 \\ i_3 \end{bmatrix} \qquad \vec{u}_{ref} = \begin{bmatrix} u_1 \\ u_2 \\ u_3 \end{bmatrix} \tag{3.11}$$

Thus the reference voltage for the microgrid is obtained:

$$\vec{u}_{ref}(s) = \vec{e}(s) - \vec{i}_{grid}(s) \cdot (R_s + L_s \cdot s) \tag{3.12}$$

The equations regard to the rotor dynamic behavior:

$$M_{mech} - M_{el} = \frac{1}{J} \cdot \frac{d\omega}{dt} + k_d \cdot \Delta\omega \tag{3.13}$$

The electric torque is produced by the electric output and influenced by the rotor's rotating speed, and the rotor's phase angel can be computed by integrating the rotating speed:

$$\begin{aligned} M_{el} &= \frac{P_{el}}{\omega} \\ \theta &= \int \omega \cdot dt \end{aligned} \tag{3.14}$$

The EMF vector is induced as a function of the phase angle:

$$\vec{e} = \begin{bmatrix} e_1 \\ e_2 \\ e_3 \end{bmatrix} = E_p \cdot \begin{bmatrix} sin(\theta) \\ sin(\theta - \frac{2}{3}\pi) \\ sin(\theta + \frac{2}{3}\pi) \end{bmatrix} \tag{3.15}$$

Wherein Equation (3.11), $\vec{e}$ is the induced EMF (electromotive force) in the stator windings, and the grid voltage is embodied by $\vec{e}$ and the measured current, i_{grid}. R_S represents the stator resistance, and L_S means the stator inductance in the simplified SG model. While in Equation 3.13, J is the inherent inertia amount. The mechanical damping factor, k_d, regulates the damping force value to counteracts the system oscillation. M_{el} and M_{mech} represent the machine's electrical torque and the mechanical torque respectively. At last, the simplified

mathematical SG model can be built based on the equations as Figure 3.8[10]. The reference voltage and the rotating rotor angle are forwarded to the PWM controller.

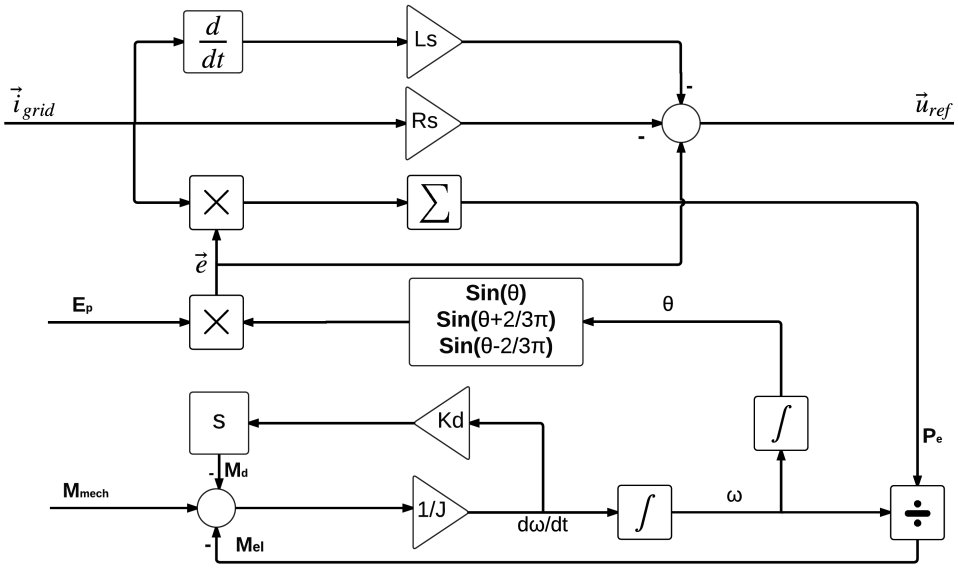

Figure 3.8: The SG model for VSG

3.4.3. ISE Lab's VSG topology

Sakimoto K, Miura Y and Ise T proposed an ISE Lab's VSG topology in [20]. Figure 3.9 [10] indicates its structure.

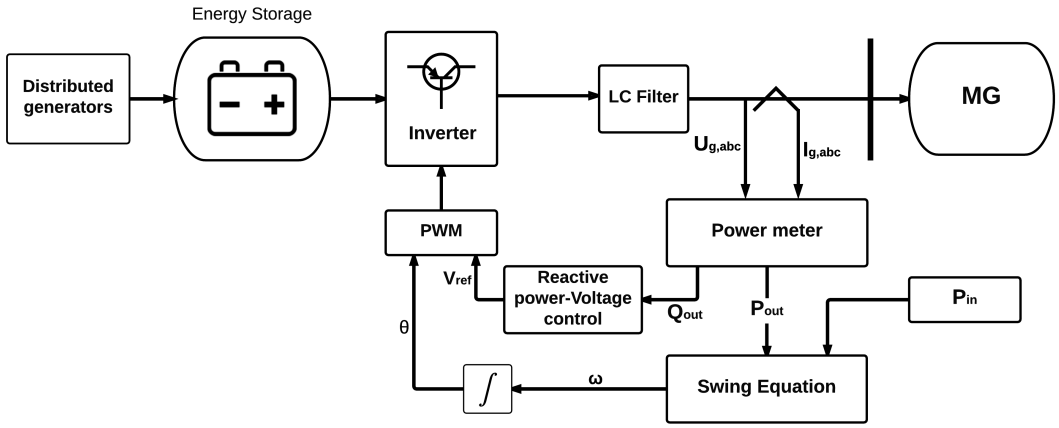

Figure 3.9: ISE Lab's VSG structure

As the Equation 3.7 explains the relationship of the VSG in/output power, the ISE's topology sets the reference input active power P_{in} and reactive power Q^*. The output power and grid frequency are calculated in the power/frequency meter. The grid frequency is obtained to compute $\Delta\omega$ (the virtual angular velocity deviation of the virtual rotor) based on Equation 3.7 by the VSG control block, and the θ (virtual mechanical phase angle) is delivered to the PWM unit in inverter as a phase command. The reference voltage value is compute by a

Proportional-Integral (PI) because usually in a MG, if the reactive power (Q) generated by the DGs increases, the local voltage should decrease, and vice versa (also, there is similar behavior for frequency verse real power (P)).

$$\begin{aligned} \Delta\omega &= \omega - \omega_0 = -R_P(P - P_0) \\ \Delta V &= V - V_0 = -R_Q(Q - Q_0) \end{aligned} \tag{3.16}$$

3.4.4. KHI's VSG topology

In [12], Kawasaki Heavy Industries (KHI) investigate an algebraic type model to establish a VSG control in an MG system. In this model (Figure 3.10[12]), a phasor diagram (Figure 3.11) of an SG is used compute the reference output current to guarantee a desirable operation under all kinds of load (especially unbalanced and nonlinear loads).

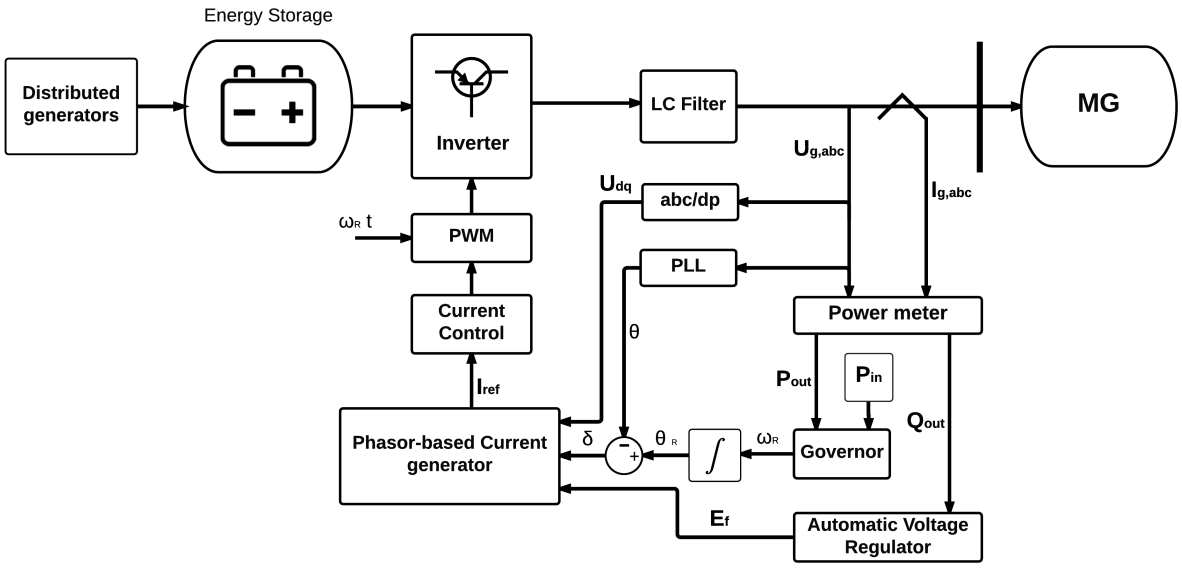

Figure 3.10: KHI lab VSG structure

$\dot{E}_f$ and $\dot{V}_g$ denote the generator's internal EMF and terminal voltage. V_d and V_q express the $d-axis$ and $q-axis$ terminal voltages, respectively, while δ signifies the internal phase angle. x and r indicates the virtual generator's synchronous reactance, armature resistance. The generator's terminal voltage and output current are measured by meters installed behind the LC filter.

According to the phasor diagram in Figure 3.11, the reference current I_d^* and I_q^* are compute as in Equation 3.17:

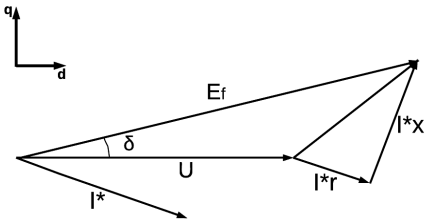

Figure 3.11: Phasor Diagram

$$\begin{bmatrix} I_d^* \\ I_q^* \end{bmatrix} = Y\left(\begin{bmatrix} E_d \\ E_q \end{bmatrix} - \begin{bmatrix} V_d \\ V_q \end{bmatrix}\right) = \frac{1}{r^2+x^2}\begin{bmatrix} r & x \\ -x & r \end{bmatrix}\begin{bmatrix} E_d \\ E_q \end{bmatrix} \tag{3.17}$$

$$E_f = |\dot{E}_f|\begin{bmatrix} sin\delta \\ cos\delta \end{bmatrix}$$

Unlike the VYSNC's topology, the PLL is used to compute the internal phase angle (δ) in the KHI's algorithm. Then the principle of the KHI's VSG is the same with others, θ (computed in swing equation) and I_{ref} are used to drive the PWM controller.

3.4.5. Overall frameworks of VSGs

In the previous sections, four addressed topologies are acquainted. According to the particular structures and requested input signal, a table is created to indicate the characteristics due to different topologies:

Table 3.1: Overall frameworks of VSGs

Algorithm	Requested signal	Addition Control loops
VSCYN's topology	Grid Voltage Battery State of Charge Virtual electromotive force Reference input power	Phase Locked Loop differential equation
IEPE's topology	Measured Current Virtual Torque, Virtual Exciting Voltage	Particular SG model
ISE Lab's topology	Grid Voltage Output Current reference reactive power reference active power	Swing equation
KHI's topology	Grid Voltage Output Current reference reactive power reference active power	Phase Locked Loop phasor-based current generator Swing equation

The swing equation plays a crucial role in the VSG control of microgrids. As shown in 3.1, the 'reference active power' or 'virtual mechanical input' is required to be set as the P_{in} in the swing equation (Equation 3.7). It applies different algorithms to regulate the inverter-side voltage, battery (energy storage system) output and also the system frequency. Since a reference input power is set to regulate the flowing energy into the grid, a current source (with computed voltage) is composed of distributed generation units, a battery and a full-bridge inverter.

3.5. Conclusions and Outlook

In this chapter, the four approaches to emulate virtual inertia in different situations are posed.

Due to the strategies that emulate virtual inertia by wind turbines and PV cells, the plan is to focus on the generation units. These methods have very targeted scopes (for the islanded microgrids supported by the wind or solar energy) and easy to be implemented (additional control signal on the MPPTs). According to the large proportion of the wind and solar power in RESs, the approaches have very broad operation scopes. Moreover, they are not influenced by the scale of MGs or the participants of any other energy sources, which could be diesel and bio-energy units. The defects are evident and mentioned in the previous section as well. It leads to an energy waste to make sure there is enough additional energy to be injected as the power of inertia. Furthermore, the extended loops (which costs money) make a lower profit and a higher opportunity for fault (more electronic components means that there are more places for fault taking place).

Concerning the virtual inertia emulation in diesel control, an amount of inertia is provided by the rotating mass of diesel engine and an ESS injects additional inertia property. Compare with the approaches for wind turbines and PV cells based MGs, the system does not cause any energy waste. Moreover, load shedding is no longer required since the combination of diesel and wind source covers all the power demand. However, it's hard to decide the size of the ESS for the ESS is merely used to store the inertia energy in short-term. And to put in the force of an extra ESS, additional control loops and inverter are needed.

With a VSG control, an ESS based islanded MG can mimic SG's dynamic behavior. The ESS and DC bus (connected with the ESS) help to manage power flow from distributed sources. Thus the grid is not affected by the variation of RESs, and the long-term storage device reduces the probability of load shedding. The problem is that the method limited by the scale of islanded MGs. The reference active power is set to regulate the energy output. If the scale of islanded MG is not large enough, it's impossible to estimate a specific value all the time.

The scopes and limitations of existing methods have been discussed. Based on the existing approaches, a method to inject inertia property in an islanded MG operates as voltage-source should be developed. And for the current-source united based MGs with diesel, the introduced approach needs to be tested and improved, and complete inverter control loops should be

proposed.

4

Proposed methods for emulation of inertia for microgrids with ESS

4.1. Introduction

Stand-still (islanded) microgrids are recommended to electrify rural area. In last chapter, the overview of the existing methods to emulate virtual inertia in current-source based islanded MGs and their operation scopes have been posed, and their the pros and cons have been discussed.

An efficient and reliable network can be realized by including long-term battery energy storage device. The operation modes is identified in Figure 2.2. Three developed methods to emulate virtual inertia property for the voltage-source based units in microgrids are developed (in order to support the demand side management). And based on the method for MGs with diesel (Figure 3.4) and the VSNYC's VSG topology (Figure 3.6), an application of PID controller for current-source units is proposed.

Thus, this chapter presents the suggested virtual inertia emulation approaches and the control loops for voltage source based systems and current-source units based grids, respectively.

4.2. Proposed methods for voltage-source based units in microgrids

4.2.1. Original control strategy

Generally in a voltage source based MG, droop control is applied for frequency and voltage regulation. It means the grid frequency is linked with the unit output active power by an

'Active power-Frequency curve', while the terminal voltage is ruled as a function of reactive power.

Active power Frequency control

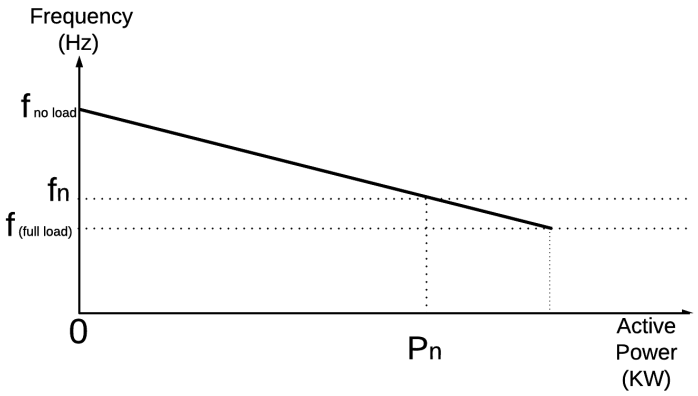

Figure 4.1: Active power-frequency curve

Figure 4.1 shows the power-frequency characteristic in droop control. In this approach frequency indicates the system power state. Figure 4.2 shows the original scheme of power-frequency control, in which Equation (4.1) is realized.

$$f_{ref} = f_n + K_f(P_n - P) \tag{4.1}$$

where the $P - f$ droop coefficient, K_f, represents the rate of the operation curve. P_n and f_n refer to the nominal value of active power and frequency. The nominal frequency value is usually set equal to that of the main grid. Form [6], the value nominal value of active power and the droop coefficient should be computed (depends on the generated RES energy and SoC of battery) by smart meters in demand side management (DSM) progress.

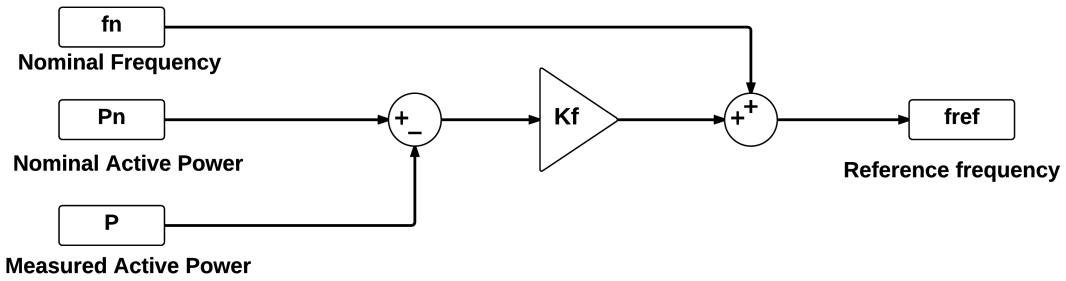

Figure 4.2: Simulink structure of Active power Frequency control

Furthermore, the frequency is set as the communication signal for demand side management, which means particular electric devices work at specific frequency [6].However, when there is a sudden change in the load side, the frequency reacts shapely. The inertia-less frequency response increase the difficulty to implement the DSM. It causes mis-operation and may do damage to the electric devices. For instance, if a large load is turned off which another one

is switched on, the inertia-less control results a rapid increase which follows by suddenly drop in frequency behavior. Some of the electricity devices will be controlled to switched on and then quickly turned off, since the devices are set to react to the change of frequency level.

To emulate virtual inertia (slow the frequency state change) in the system, three approaches are developed as follows: introducing swing equation, adding a low-pass filter and setting a rate limitation.

Reactive power Frequency control

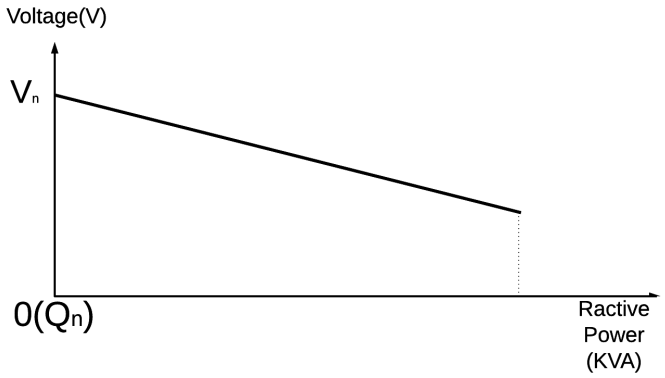

Figure 4.3: Reactive power-voltage curve

Figure 4.3 shows the reactive power-voltage curve in droop control. In this approach, grid voltage is used to express the load reactive demand. Equation (4.2) describes the applied function.

$$V_{ref} = V_n + K_q(Q - Q_n) \tag{4.2}$$

K_q keeps a constant value which is regarded as the $Q - V$ droop coefficient, and it sets the deviation rate when the grid voltage is oscillating around its nominal point.

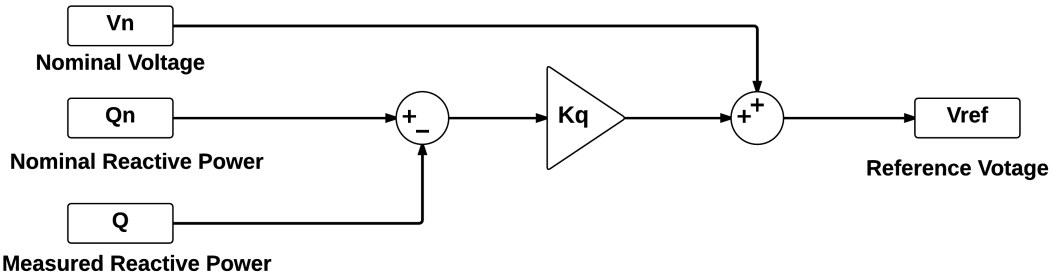

Figure 4.4: Simulink structure of Reactive power Voltage control

With the presented controllers, the active output is expressed by the frequency, while the voltage value is related to the reactive output. In this way, the grid state is completely described by a voltage signal since the voltage-source unit is the only energy supplier in the investigated system.

4.2.2. Approach i: introducing swing equation

In $chapter\ 3$, existing methods to emulate virtual inertia, adding swing equation (Equation (3.7)) is regularly regarded as a solution to imitate inertia property. The difficulty in importing swing equation is that the input/output power of a voltage source remains equal to the load, which means the power balance in a voltage-source based unit could be expressed as the Equation (4.3).

$$P_{in} = P_{out} = P_{load} \tag{4.3}$$

With this feature, there is no controller to govern the output of the BESS and it merely follows the real-time value of energy demand. Therefore, the swing equation is introduced based on an assumption, which is to define a virtual power from inverter side. The virtual power should be coupled with the output frequency, as the relationship between generated power and the rotating rotor in a synchronous machine [21]. In the accordance with the original droop control scheme, the defined virtual input power is transformed from Equation (4.1):

$$\begin{aligned} f &= f_n + K_f(P_n - P_{grid}) \\ P_{in} &= (f_n - f)/K_f + P_n \end{aligned} \tag{4.4}$$

where P_{in} is the identified as the virtual input from the inverter side. Its variation is restrained by the system frequency and it keeps equal to (or moving towards) the load value. It's able to involve swing equation after obtaining P_out from a grid side power meter. Based on Equation (4.4), swing equation can be involved in the droop controller.

$$\begin{aligned} P_{in} - P_{out} &= K_i \frac{df}{dt} \\ f &= f_0 + \int k_i(P_{in} - P_{out}) \\ (k_i &= \frac{1}{K_i}) \end{aligned} \tag{4.5}$$

where K_i is regarded as the inertia coefficient, which describes the injected inertia quantity. The inertia coefficient k_i is acquired by a reciprocal function of the injected inertia K_i, and acts a speed limitation for the frequency deviation per unit time which is a response to the change of active power. The smaller k_i is, the frequency response is slower and larger inertia is achieved. Combine Equation (4.4) and (4.5), the formula of preferred frequency is indicated as:

$$f = f_0 + \int_0^t k_i((f_n - f)/K_f + P_n - P_{out})dt \tag{4.6}$$

According to Equation (4.6), the droop control loops has been expanded by the introduction

of swing equation. The $P-f$ coefficient, K_p, acts to impact an equal reaction of frequency to the change of active power as the original control scheme. The integral progress makes the frequency behavior become a function of both active power (P) and time (t). The structure of the new control loop is indicated in Figure 4.5.

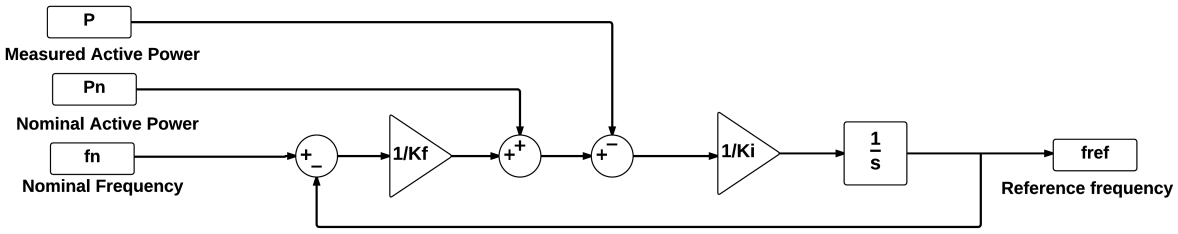

Figure 4.5: PF droop control scheme with swing equation

As the only energy source in the isolated MG, BESS dominates the operating frequency via the included inverter. The feedback process can be directly implicated by the computed value from the control loop. The reference frequency value is directly delivered to the PWM controller which decides the grid frequency.

4.2.3. Approach ii: placing low-pass filter

The main target is to improve the system frequency behavior, which could be removing harmonics, cutting down (or remove) the overshoots and smoothing its dynamic behavior. By inserting a low-pass filter for the reference frequency of inverter control, the required impact could be achieved. The low-pass filter should be set in front of the reference frequency block as shown in Figure 4.6 (The additional control process is highlighted).

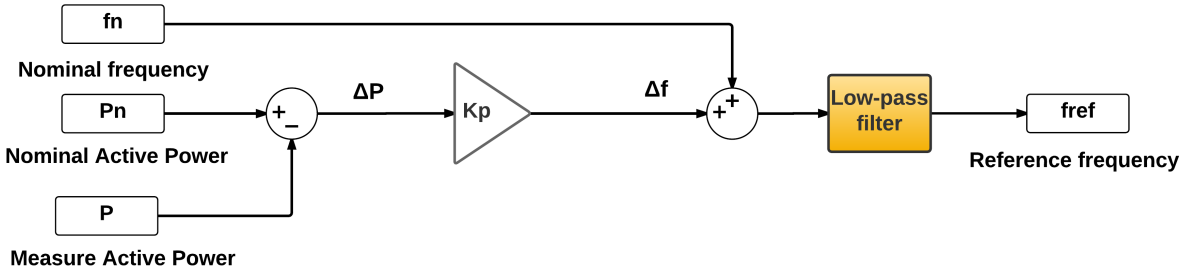

Figure 4.6: PF droop control with Low-pass filter

The transfer function of low-pass filter to regulate the frequency is:

$$H(s) = \frac{1}{ks+1} \tag{4.7}$$

Express the transfer function with state space representation:

$$x' = -\frac{1}{k}x + \frac{1}{k}$$
$$y = x \tag{4.8}$$

As shown in the state space representation in Equation (e Vsf3), it's a $1st$ order function with 1 input and 1 output. Since the input signal represents the grid frequency, x oscillates around its nominal value (50Hz). Therefore, the frequency changing rate , x', is restrained by the setting value of k. After the Laplace inverse transformation, the gird frequency is computed as:

$$f_{ref} = f_0 + (f(t) - f_0)(1 - e^{-\frac{1}{k}t}) \tag{4.9}$$

In Equation (4.9), when the coefficient k is comparably small, the filter works as a filter to remove harmonics, and coefficient k represented a 'cut down' frequency value. If setting a higher value of k, a time delay is introduced to the frequency performance, which could provide an outcome similar to that of $Approach\ a$.

4.2.4. Approach iii: setting rate limitation

A Rate-Limitation control can be used to implicate the frequency behavior as well. The The function of a $RateLimiter$ is to limit the rate of change of a signal. The derivative rate of the passed signal is calculated by:

$$r = \frac{u(i) - y(i-1)}{t(i) - t(i-1)} \tag{4.10}$$

where $u(i)$ and $t(i)$ means the block's current input and time, while $y(i-1)$ and $t(i-1)$ are the block's output and time at the previous step.

The first derivative of the signal is restricted by comparing the computed $rate$ to the setting rising slew rate (R) and falling slew rate (F). Unlike the responses with the additional filter introduced in $approach\ ii$, the rate limiter has a non-linear behaviour.

- When the calculated r is higher than R, the output is regulated as:

$$y(i) = \Delta t \cdot R + y(i-1) \tag{4.11}$$

- When the calculated r is smaller than R, the output is commanded as:

$$y(i) = \Delta t \cdot F + y(i-1) \tag{4.12}$$

- When the r is between R and F, the output is equal to the input signal:

$$y(i) = u(i) \tag{4.13}$$

In this way, a limitation (from minimal several thousandths to maximum a few hundred) of the change of rate of frequency (RoCoF) is established for the network. And the control mechanism is displayed in Figure 4.7 (The additional control process is also highlighted).

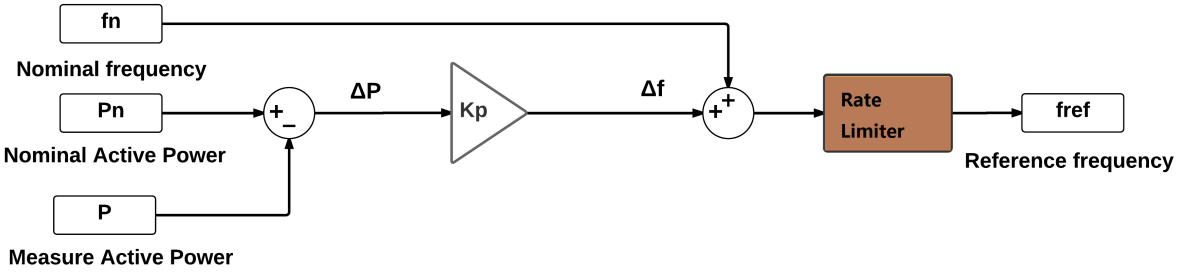

Figure 4.7: PF droop control with a Rate Limiter

The advantage of the Rate Limiter is that the RoCoF can be rigid restrained, and the frequency deviation time is directly proportional to the load change.

4.3. Proposed methods for current-source based units in microgrids

The participation of RESs DGs (which have either very low or no rotating mass) degrades the inertial level of the whole network and results to revere impacts in power system stability. In the previous chapter, the power electronics methods to enhance system reliability is introduced. Depend on the additional control loops existing approaches, a P(I)D controller is proposed for the investigated MGs which equipped with battery long-term storage system.

4.3.1. Original strategy

Customarily, RESs generators do not participate in securing system stability or providing inertia ability. The preferred battery storage system output signal, usually decided by the locate weather (which determines the timely RES generation) and the state of charge of battery, is delivered to a power control strategy in the inverter of a current-source network. The reference output value may stay constant for a long period until the battery SoC changes into another state. The structure can be simply stated by the structure in Figure 4.8.

In Figure 4.8, P_{ref} is the preferred output power from the current source with a device for energy storage (generally a battery). It extents the size of the MG without providing inertia property and may result in system instability.

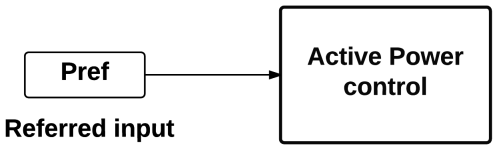

Figure 4.8: Original current-source power control

4.3.2. Virtual inertia emulated by a PID controller

In the Section 3.3, a plan to virtual inertia emulation in a diesel-wind MG is stated. And the VSYNC's VSG topology introduces the idea of adding differential function in long-term storage system and the application of additional damping force. Combine the two methods, an extra P(I)D (proportional, integral, and derivative) control is proposed for the investigated current-source based MG with diesel. In this case, the integral function in the PID control is not required. The structure of extra loops is shown in 4.9.

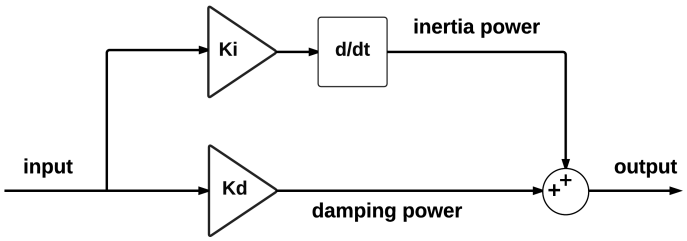

Figure 4.9: Structure of PID controller

In this way, the reference energy transmitting value for the current source is kept resetting as a function of the deviation frequency:

$$\begin{aligned} \Delta f &= f_{grid} - f_{nominal} \\ P_{ref} &= P_n + K_i \frac{\Delta f}{dt} + K_d \Delta f \end{aligned} \tag{4.14}$$

where P_n is the preferred output power from the current source with a device for energy storage (generally a battery). It renders the standard operation situation of a current source, and the value is decided by the state of charge of the battery and the quantity of generated RES energy. The secondary part of the equation represents the injected inertial power, and K_i means the inertia mass. The effect of damping force (Figure 4.10) could be discerned for it has not been considered in [13]. Figure 4.10 the proposed control loop depends on the Equation 4.14.

The flowchart (Figure 4.11) describes the operation process in this approach. A dead zone is applied to this method for there is no need to react to minuscule disturbances.

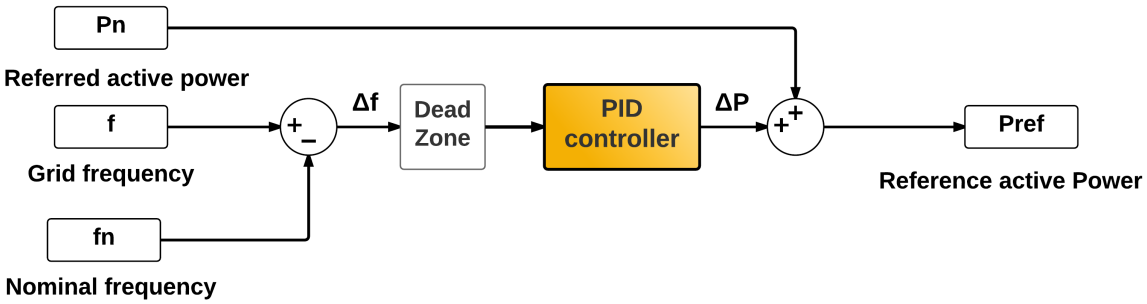

Figure 4.10: Emulate inertia with PID controller

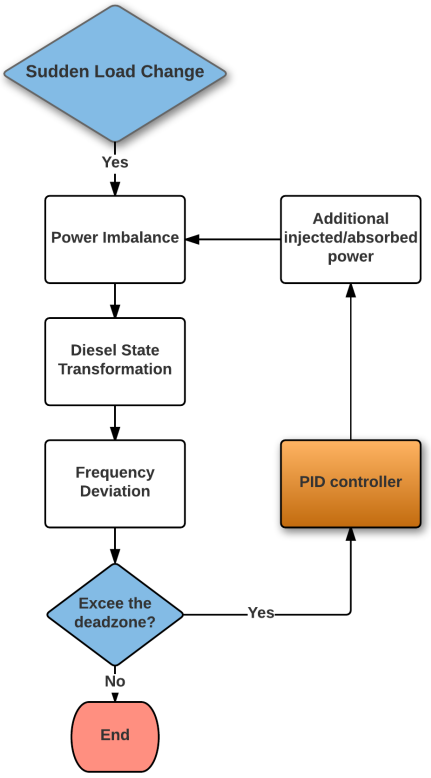

Figure 4.11: Virtual inertia emulation process in current-source and diesel based units

5

Case studies

5.1. Introduction

In this chapter, the case studies of investigated MG systems are explained.

Due to the proposed three mechanism schemes to improve the frequency response in voltage-source units based MG, different scenarios, which aim to test and analysis the suggested approaches, are described. A MG with the capacity of 100MW is modeled for the case with voltage-source based unit. And the BESS supplies all the electricity load in the system.

The BESS in the current-source based MG also covers around 100MW when the load demand reaches 200MW. A diesel engine is applied to cover the rest of the load and the sudden incident (load change). The situations of the implementation of PID controller to emulate virtual inertia are established. At last, the comparison aspects between the voltage source based MG and the current source based MG are described.

5.2. Case study A: voltage source inverter - islanded microgrid

5.2.1. Case description

Table 5.1 gives a description of investigated islanded microgrid in Case A. The regular operation state and the largest incident are indicated. In this pure RESs situation, the battery storage system is the only supplier in the grid, and the inverter dominates frequency. Frequency is used as the communication signal for the demand side management in the voltage-source units based MG (particular electric devices operates in specific frequency arrange [6]). Thus, the active power - frequency control is implemented in the network, which embodies a grid frequency ruled by a $P-f$ curve. Equation 4.1 and Figure 4.2 presents the explanation of the

droop control system.

RESs Source Type	Voltage Source
Load	100 KW
Active Power from RESs	100 KW (1 p.u.)
Largest Load Change	+50 KW (0.5 p.u.)
Inverter Control	Droop Control
Frequency	Inverter Dominates

Table 5.1: Microgrid characteristics for Case A

5.2.2. Scenario description: voltage source inverter - islanded microgrid

The scenarios in $Case\ A$ include the operation behaviors of the voltage source inverter - islanded microgrid in different conditions. The scenarios are described as follows:

- The original control strategy should be tested before attaching the loops for frequency improvement. $Scenario\ a.1$ consists various amount of disturbances (load change) and review the impact of droop factor K_f. In this scenario, three different value of disturbances, $0.3pu$ $0.4pu$ and $0.5pu$, are injected to the investigated network. Since the droop factor (K_f) is set by the demand side control, the behavior due to droop factor adjustment should be included. The situations with $K_f = 0.2$ and $K_f = 0.4$ are considered.

- $0.5pu$ is the reviewed largest disturbance, and it's regarded as the typical event. $Scenario\ a.2$ imitates the situation when droop control loops are transformed by the injection of swing equation. The impact of the implicated control loops are tested with three different values of inertia coefficient ($k_i = 3e^{-3}$, $5e^{-4}$,and $7e^{-5}$). And the responses introduced by different droop coefficient value (0.2 and 0.4) are compared.

- $Scenario\ a.3$ indicates condition the system frequency dynamic behavior regulated by a low-pass filter. The system behaviors are observed by setting the time coefficient to 0.01, 0.08 and 0.16, respectively. The performances with droop coefficient adjustment (0.2 and 0.4) are involved as well.

- The effects by implementing rate limiter are addressed in $Scenario\ a.4$, three rate limitations ($R = 1.5$, 2.5,and 3.5) are applied to explain its influences in system frequency response. Due to $R = 1.5$, the network behavior are displayed with the change of the droop coefficient (from 0.4 to 0.2).

- By adjusting the related coefficients, the same frequency deviation period can be realized in the systems with the three developed methods. In this situation, the approaches can be compared. And the combination of two approached could be tested.

5.3. Case study B: islanded microgird with diesel

5.3.1. Case description: current source inverter - islanded microgrid

Table 5.2 explains the operation condition and the sudden load change of the current source based MG. The given information describes the situation that the load excesses the capacity of the RESs and a diesel engine is taken out as an extra source to supply the rest of the electric demand. The occurrence is selected similarly to the incident in $Case\ A$.

RESs Source Type	Current Source
Load	200 KW
Active Power from RESs	100 KW (0.5 p.u.)
Active Power from Diesel	100 KW (0.5 p.u.)
Largest Load Change	+100 KW (0.5 p.u.)
Inverter Control	PQ Control
Frequency	Diesel Dominates

Table 5.2: Microgrid characteristics for Case B

5.3.2. Scenario description: current source inverter - islanded microgrid

Scenarios in $Case\ B$ holds the assumptions in the current source inverter connected islanded MG with a diesel engine.

- $Scenario\ b.1$ is composed of the frequency responses without BESS participation. Various disturbance amplitudes ($0.15pu$, $0.25pu$ and $0.5pu$) are brought to the isolated MG system.
- The grid inertia level is enhanced by the additional power supply from BESS, which is realized by a derivative equation in the PID controller. In the $Scenario\ b.2$, the damping factor, K_d, is set to 0, and the system correlated behaviors are tested with the inertia factor K_i equals to 1000, 2000, and 3000.
- The influences of the injection of the damping force by BESS are experimented in the $Scenario\ b.3$. The damping factor is set as $K_d = 1$, 2, and 3 while the inertia factor is controlled to be 0. All the responses with BESS participate to enhance grid stability should be compared to the original performance which without BESS involved.

5.4. Case study C: voltage-source and current-source based MGs

This scenario includes the comparison between the islanded network without and with a diesel engine. The status is classified by two of the most essential elements, the active power and the frequency, as follows:

- The power behaviors in the MG without diesel and with diesel (with and without the BESS support) should be distinguished. In $Scenario\ c.1$, the income disturbance level in the two systems are set to the same ($0.5pu$). Since the developed approaches do not influence the power activity in voltage-source based MG, the performance of voltage source should be compared to the supply of current-source based MG with and without the addition PID controller participation.

- $Scenario\ c.2$ presents the difference among the frequency responses in the voltage-source based MG (without and with the additional control schemes) and the current-source based MG with diesel (with and without the BESS participation in the inertia emulation). In detail, the frequency deviations are adjusted to be the same (by fixing the value of droop coefficient K_f) in both of the system with the original control schemes. Then, the effects of the proposed control loops are listed to compare with the original responses.

6

Modeling

6.1. Introduction

Corresponding Simulink models are presented for each of the elements. In a dual modeling approach, a voltage-source units based MG and an MG supported by a current-source units with diesel have been modeled separately. The original controllers and the systems with addition inertia control loops are presented.

6.2. Modeling for Case A

An overview of the invested microgrid system configuration and control structure is displayed by Figure 6.1:

As shown in the structure, the battery (at the right-bottom of the diagram) becomes the only energy source in the MG, and it's directly connected to a three phase full-bridge inverter. In this case study, there is no need to consider the state of charge (SoC) of battery because due to a sudden load change the investigated period is in milliseconds. The supplied electric power flows in the grid through an LC filter, which regulars the shape of the output signal. The left part of Figure 6.1 illustrates the draft of the inverter controller. The voltage and current signal, which measured from the grid side, are transformed from the a, b, c sequence to $d, q, 0$ sequence to compute the active & reactive power, which are utilized as the input signals in the voltage control and current control. The reference voltage for the PWM generator is produced via the voltage control and current control because the shape and value of the voltage are of a dramatic difference between before and the LC filter and the output current also affects the PWM signal. In the particular model, an additional scope is placed to observe the behavior of active power and frequency.

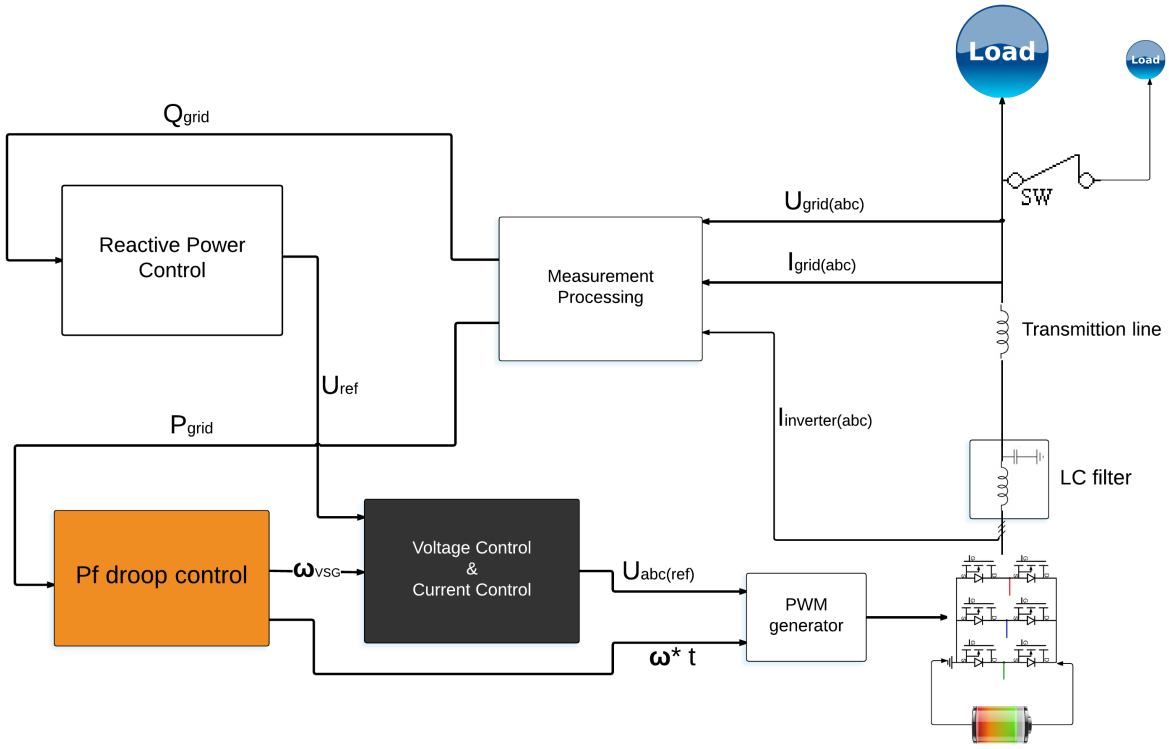

Figure 6.1: Overview of the voltage-source units based microgrid configuration

The droop control schemes and the developed methods have been demonstrated in the last chapter. All of the developed methods (approach a, b and c) can be implemented and tested in the Pf droop control scheme (The orange block in Figure 6.1).

6.2.1. The measurement process

The $dq0$ Transformation

A abc to $dq0$ transformation blocks are placed in the measurement process. The effect is to remove the time-dependent coefficients. The transform matrix is defined as:

$$A = \begin{bmatrix} cos\Theta & -sin\Theta & 1 \\ cos(\Theta - \frac{2\pi}{3}) & -sin(\Theta - \frac{2\pi}{3}) & 1 \\ cos(\Theta + \frac{2\pi}{3}) & -sin(\Theta + \frac{2\pi}{3}) & 1 \end{bmatrix} \tag{6.1}$$

$$A^{-1} = \frac{2}{3}\begin{bmatrix} cos\Theta & cos(\Theta - \frac{2\pi}{3}) & cos(\Theta + \frac{2\pi}{3}) \\ -sin\Theta & -sin(\Theta - \frac{2\pi}{3}) & -sin(\Theta + \frac{2\pi}{3}) \\ \frac{1}{2} & \frac{1}{2} & \frac{1}{2} \end{bmatrix}$$

The relation between the old variables and the new variables (e.p. the terminal voltage V_g and V_g') is:

$$\begin{aligned} \dot{V}_g &= A \cdot \dot{V'}_g \\ \dot{V'}_g &= A^{-1} \cdot \dot{V}_g \end{aligned} \tag{6.2}$$

where:

$$\dot{V}_g = \begin{bmatrix} V_{g,a} \\ V_{g,b} \\ V_{g,c} \end{bmatrix} \quad and \quad \dot{V'}_g = \begin{bmatrix} V_{g,d} \\ V_{g,q} \\ V_{g,0} \end{bmatrix} \tag{6.3}$$

And the required phase angle signal can be computed by the frequency signal from the droop controller frequency output or from a PLL measurement (They share the same value for they represent the reference frequency for the inverter and the system frequency, which is dominated by the inverter).

$$\begin{aligned} \omega &= f \cdot 2\pi \\ \Theta &= \omega \cdot t \end{aligned} \tag{6.4}$$

In this case, the signals of terminal voltage (V_g), current (I_g) and the inverter output current (I_c) are sent to the 'abc to $dq0$' transformation blocks.

Active and Reactive power measurement

As indicated in Equation 4.1 and 4.2, the preferred frequency value is computed by the $P-f$ droop curve, and the voltage value is related to the reactive output. The output power of the BESS is estimated by the measured grid-side voltage and the flowing current (Equation (6.5), (6.6)).

Active Power:

$$P_{out} = U_d I_d + U_q I_q \tag{6.5}$$

Reactive Power:

$$Q_{out} = U_q I_d - U_d I_q \tag{6.6}$$

where the $U_{d,q}$ and $I_{d,q}$ are the $dq0$ sequences of the grid side voltage and current, which are converted in the abc to $dq0$ transformation block. And the control mechanism is distinct (shown in Figure 6.2).

The obtained results become the source of income signals of the droop control in Figure 4.2 and 4.4.

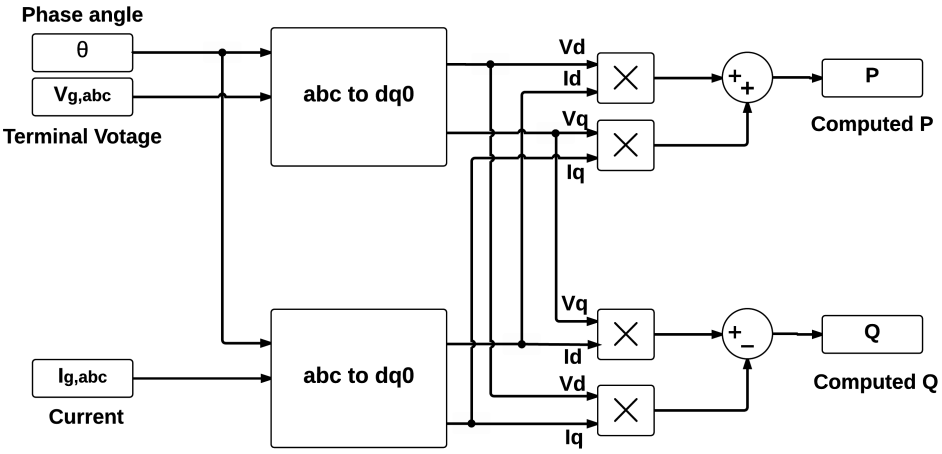

Figure 6.2: Algorithm to compute active and reactive power

6.2.2. Voltage control and current control

Voltage control

The aim of voltage control is to compute the reference current value of inverter output (i). The dynamic equation of current (AC side) can be expressed as [21]:

$$i = i_g + \omega C U_g \tag{6.7}$$

where i_g refers the current value flows into the grid (load). To work for both of the active/reactive power, park transformation is required. And the equation becomes:

$$\begin{aligned} C\frac{dU_d}{t} &= i_d - \omega C U_q \\ C\frac{dU_q}{t} &= i_q - \omega C U_d \end{aligned} \tag{6.8}$$

According to Equation (6.8), the voltage control loops is shown in Figure 6.3 [22]

where k_{pv} and k_{iv} are the proportional and integral gains in the PI controllers. The obtained reference values are directly delivered to the current control scheme.

Current control

The introduced current control (CC) is also called the inter current control loop. Base on Figure 6.1, the dynamic equation of voltage (AC side) can be expressed as [21]:

$$L\frac{di_l}{dt} = -R_s i_l + V_g - V_i \tag{6.9}$$

where L_f means the filter inductance, i_l refers the flowing current in the inductance and R_s is the equivalent resistance. Via park transformation (introduced in the previous part), the Equation (e droopC1) becomes:

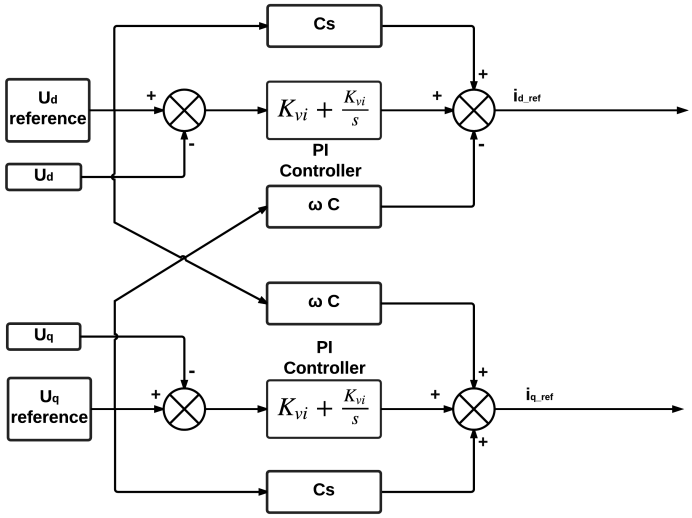

Figure 6.3: Voltage control strategy

$$L\frac{di_d}{dt} = -R_s i_d + V_d - V_{i,d} + \omega L i_q$$
$$L\frac{di_q}{dt} = -R_s i_q + V_q - V_{i,q} - \omega L i_d \tag{6.10}$$

where $\omega L i_q$ and $\omega L i_d$ are coupling terms. Based on Equation (6.10), the current control loops can be modeled as Figure 6.4 [22]

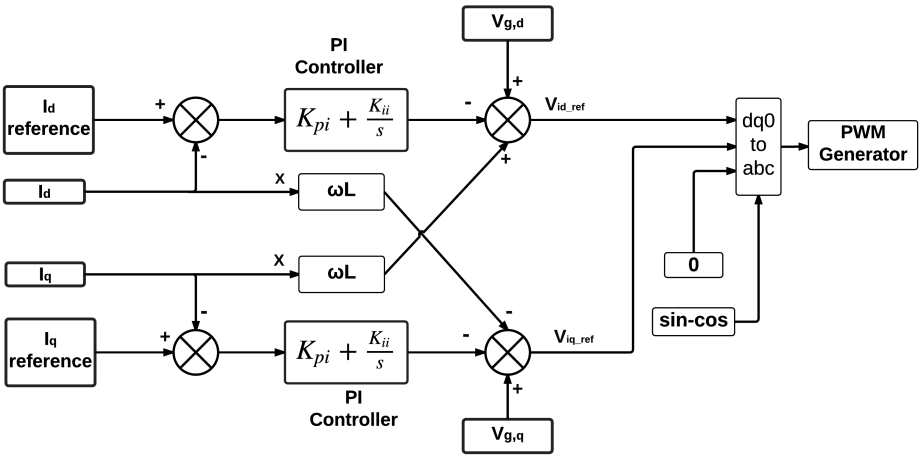

Figure 6.4: Current control strategy

where k_{pi} and k_{ii} mean the proportional and integral gains for the PI controllers in current control. The output signal is the reference voltage value at inverter side.

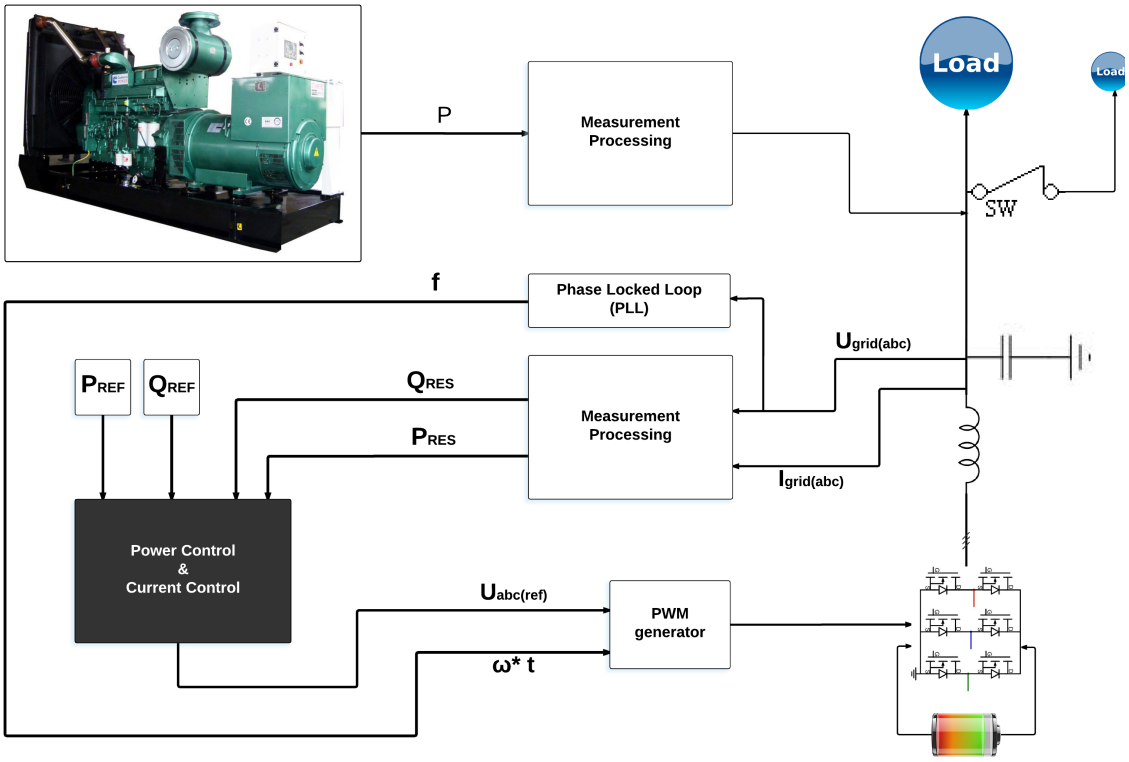

Figure 6.5: Overview of the current-source units based microgrid configuration

6.3. Modeling for Case B

Figure 6.5 exhibits the structure of the current source and diesel based MG (the effect of the transmission line is neglected). As can be seen in the diagram, the main construction is very familiar with the voltage source based MG, which is displayed in Figure 6.1. Diesel is used to maintain the islanded MG. It's noticeable that the system frequency is linked to the rotor's rotating speed in the diesel engine, while the inverter output is controlled to follow the frequency signal (provided by a Phase Locked Loop). And a PQ power controller is put in practice to regulate the BESS output as stated Subsection 4.3.1.

The transformation between the $dq0$ sequence and abc sequence is introduced in Subsection 6.2 and the measurement progress in these two cases are the same. The PLL block is from the Simulink Library, which is used to computing the network frequency of the input signal and traces the phase angle.

6.3.1. Diesel

The behavior of diesel is simulated by a simplified synchronous machine block which is also included by Simulink Library. Both of the electrical and mechanical characteristics of a particular synchronous machine are modeled. And the mechanical system is described by:

$$\Delta\omega(t) = \frac{1}{2H}\int_0^t (T_m - T_e)dt - k_d\Delta\omega(t)$$
$$\omega(t) = \Delta\omega(t) + \omega_0 \tag{6.11}$$

where $\Delta\omega$ is the speed variation with respect to speed of operation. H means the inherent inertia of the SG. T_m and T_e represent the mechanical and electric torque respectively. And k_d stands for the damping force as introduced in the previous chapters.

6.3.2. Active power and reactive power control

The active power and reactive power (PQ) control is also called the active power control (PC) and current control (CC) for the reference voltage comes from the grid side. Set the grid voltage on q sequence equal to zero, which means:

$$U_q = 0 \tag{6.12}$$

Put Equation 6.12 into Equation 6.5 and 6.6. Thus:

$$P_{ref} = U_{gd}i_{gd}$$
$$Q_{ref} = -U_{gd}i_{gq} \tag{6.13}$$

By transforming the Equation 6.13, the reference of grid flowing current is obtain:

$$i_{gd\_ref} = \frac{P_ref}{U_{gd}}$$
$$i_{gq\_ref} = -\frac{Q_ref}{U_{gd}} \tag{6.14}$$

Therefore, the power control loop where aims to obtain the reference current value is established in Figure 6.6.

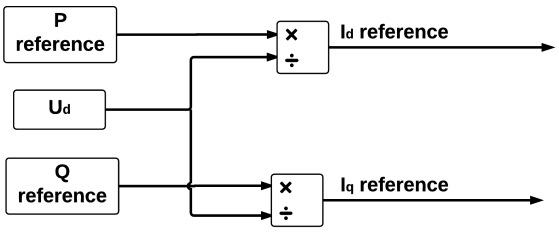

Figure 6.6: Power control

The compute reference grid signals are sent to the inter current control (CC) loops. The principle of the current control is the same with the one in voltage-source control scheme. PI controllers are also applied to calculate the inverter side reference voltage (d sequence and q sequence, respectively). However, it's importance to know the investigated current is from

the grid side, the decouple terms (ωLI) will be from the impedance in the transmission line.

6.3.3. Virtual inertia emulation in Case B

Considering the control schemes to emulate virtual inertia in the MG, the VSG control, which has been discussed in Section 3.4, can not be implemented. The VSG control mimics synchronous machine models' the power and frequency responses. Compare to an inverter, the frequency of diesel output is different to monitor and insensitivity to react. VSG control could result in conflicts between two frequency source and unnecessary oscillations. The appropriate electronic method, an additional PID controller, is addressed in Subsection 4.3.2. The new strategy after applying the PID control is presented in Figure 6.7.

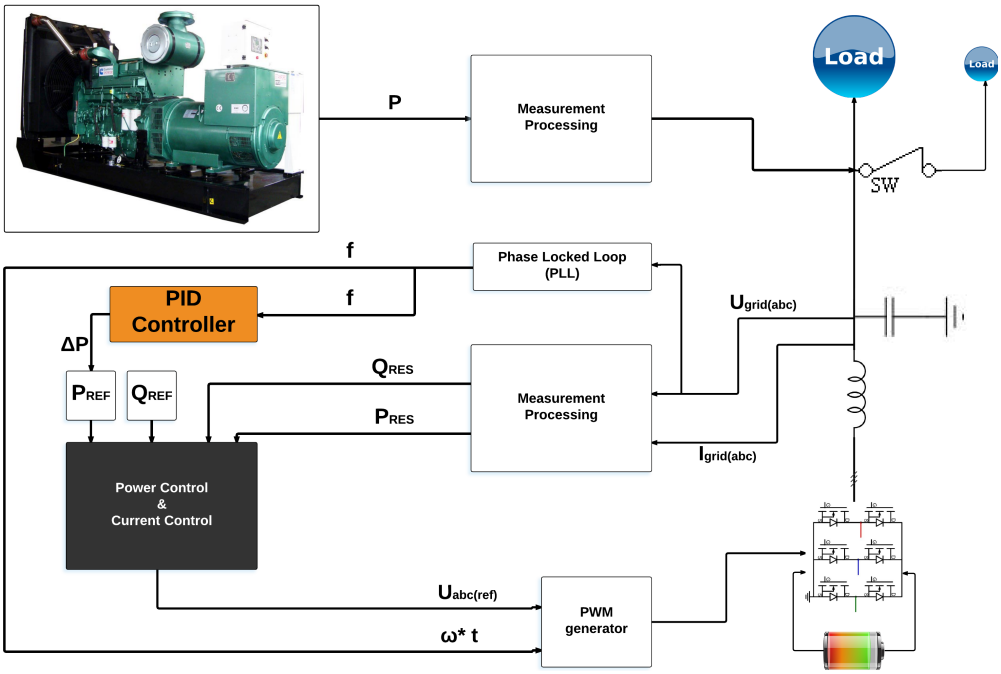

Figure 6.7: Inject virtual inertia to the current source based microgrid

6.4. Parameters for modeling

The parameters for voltage-source units based case are shown in Table 6.1. And Table 6.2 displays the parameters for current-source units based MG network. Some of them and initial inputs depends on the model in [22], and the others got adjusted by testing in the Simulink model.

Table 6.1: Parameters for modeling the voltage-source units based MG

Microgrid:				
Par.	U_{dc}	L (filter)	C (filter)	Line
Value	$1000V$	$800\mu H$	$500\mu F$	Ignored
Droop:				
Par.	P_n	Q_n	f_n	U_n
Value	100KW	0KW	50Hz	380V
VC & CC:				
Par.	k_{pv}	k_{iv}	k_{pi}	k_{ii}
Value	10	2000	0.5	0

Table 6.2: Parameters for modeling the current-source units based MG

Microgrid:				
Par.	U_{dc}	L (filter)	C (filter)	Line
Value	$1000V$	$800\mu H$	$500\mu F$	$5Ohm$ $50e^{-6}H$
Diesel:				
Par.	P_n	V_n	f_n	H
Value	200KW	380V	50Hz	3.5
PC & CC:				
Par.	P_{ref}	Q_{ref}	k_{pi}	k_{ii}
Value	100KW	0KW	0.5	20

7

Simulation Results

7.1. Introduction

The principles of inverter control with and without special inertia emulation circuits are introduced in $Chapter\ 4$. In this chapter, the simulation results of the defined cases (identified in $Chapter\ 5$) are presented and discussed. The dynamic models (introduced in $Chapter\ 6$) of the investigated networks are implemented in the MATLAB Simulink.

7.2. Simulation results: islanded microgrid without diesel

7.2.1. Scenario a.1: original droop control

Voltage and current signals

The propose of this scenario is to check the established model of the voltage-source based MG, in which a droop control is implemented for the inverter. An incident (0.2 p.u. load change) occurs at time $t = 0.3$ and switches off at $t = 0.8$ (The simulation will only focus on the first disturbance from the next scenario for the entirely relative reaction). The grid-side voltage and current are measured by electricity meters as shown in Figure 7.1. The measured power is obtained via a first order filter with a $2000Hz$ cut-down frequency, which aims to remove the noise.

As the outcome from the voltage and current meters, the signals become sinusoidal via passing the LC filter. The voltage signal peaks at $312V$, which corresponds a virtual value of $220V$ and a $380V$ line-to-line voltage. It follows the design in Table 6.1. The nominal system voltage keeps unchanged as the output of reactive power (generally, the voltage derivation is not evident in an MG in which droop control is applied to the inverter). When there is a disturbance in

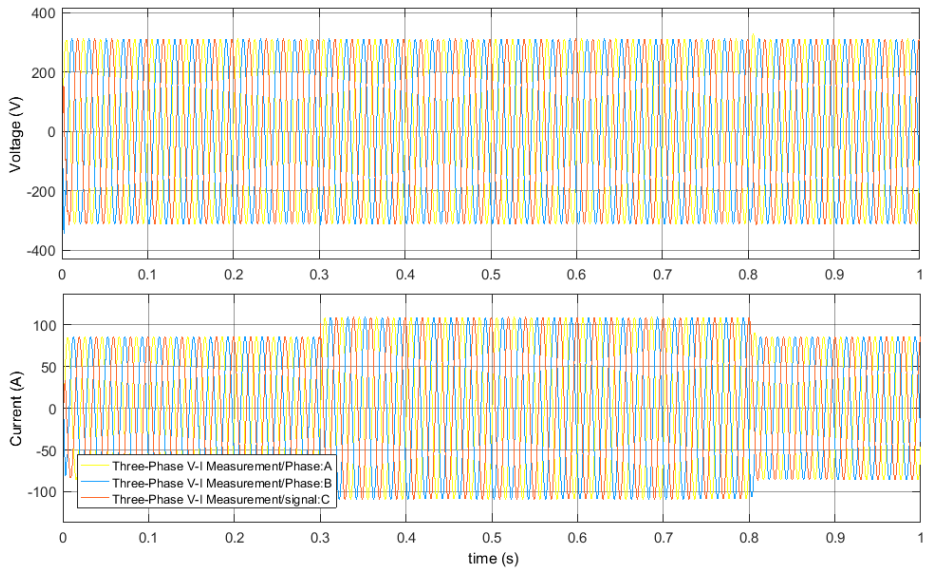

Figure 7.1: Scenario a.1: Voltage and current signals in electricity meter

the system (as shown at $t = 0.3,\ 0.8$), the current reacts immediately to complete the state change.

Change in disturbance

To examine the droop property in frequency performance, three particular additional loads ($0.3\ 0.4\ 0.5\ p.u.$) are injected and called off into the system. The droop coefficient, K_f, is fixed to 0.4 in these tests. Figure 7.2 presents the dynamic responses of the specific events. The system frequency deviates directly proportional to the power change. And the results match the computed expectation. The largest introduced disturbance, $0.5\ p.u.$, is picked for the further simulations.

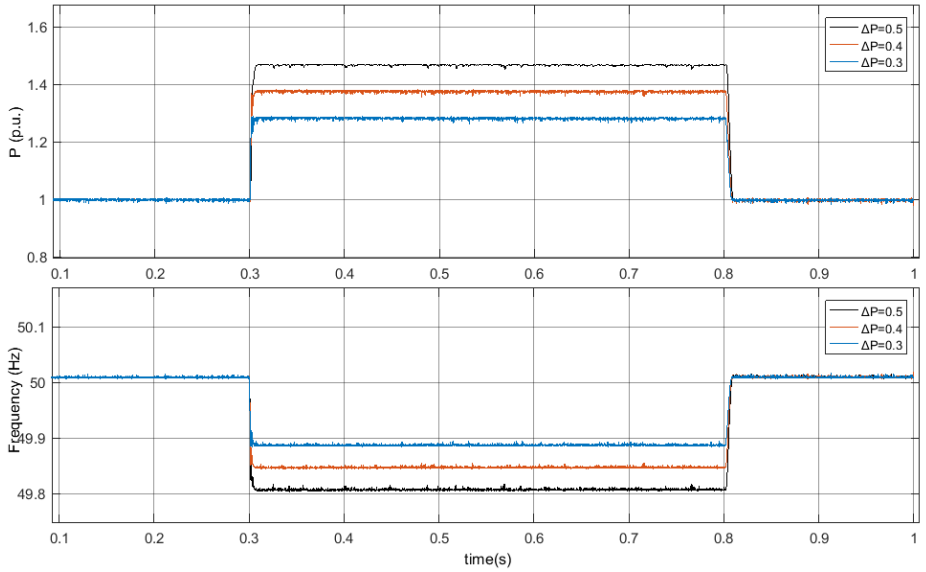

Figure 7.2: Scenario a.1: Frequency responses due to different disturbances

Change in droop coefficient, K_f

Equation 4.1 indicates that the frequency response is also related to a coefficient, K_f, which decides the rate of a P-f curve. As mentioned in earlier, the frequency differs proportional to the load change. K_f describes the dimension of the magnification. Figure 7.3 shows the performances with various K_f. $K_f = 0.4$ is selected for the normal state, and a smaller $K_f = 0.2$ is used as a comparison in the other cases. And it's also can be seen in the figure, the change of rate of frequency is extremely high (60Hz/s), which gives reason why inertia property in frequency response is required.

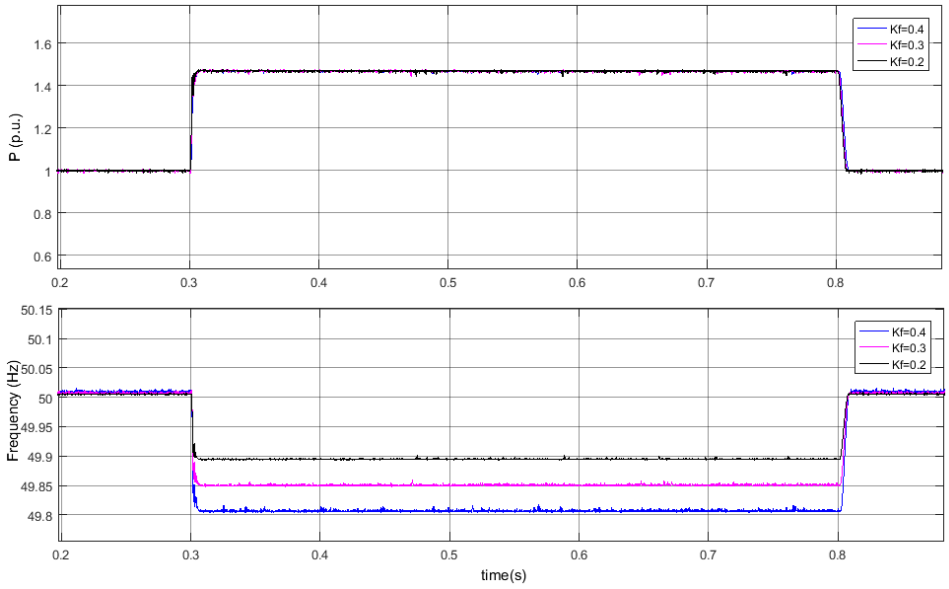

Figure 7.3: Scenario a.1: Frequency responses due to different K_f

7.2.2. Scenario a.2: introducing swing equation

The first approach to emulate virtual inertia is to bring the swing equation. A virtual input is assumed, and an inertial function is installed between the virtual power and the load. Equation 4.5, 4.6 and Figure 4.5 give fully explanation on how it works.

Change in inertia coefficient, k_i

By bringing in the swing equation, the frequency output is determined by an inertia coefficient k_i and the power demand, and it works as a function of time because of the integrated term (explained in Equation (4.6)). Figure 7.4 displays the dynamic responses due to k_i with different values.

From the shown results, the frequency behavior is considerably improved for there is not harmonics or overshoots anymore. Moreover, the approach makes the performance more controllable and reliable, e.p. if a fault occurs in the MG, the method provides time for the protection device and avoid the misoperation by the demand side management plan.

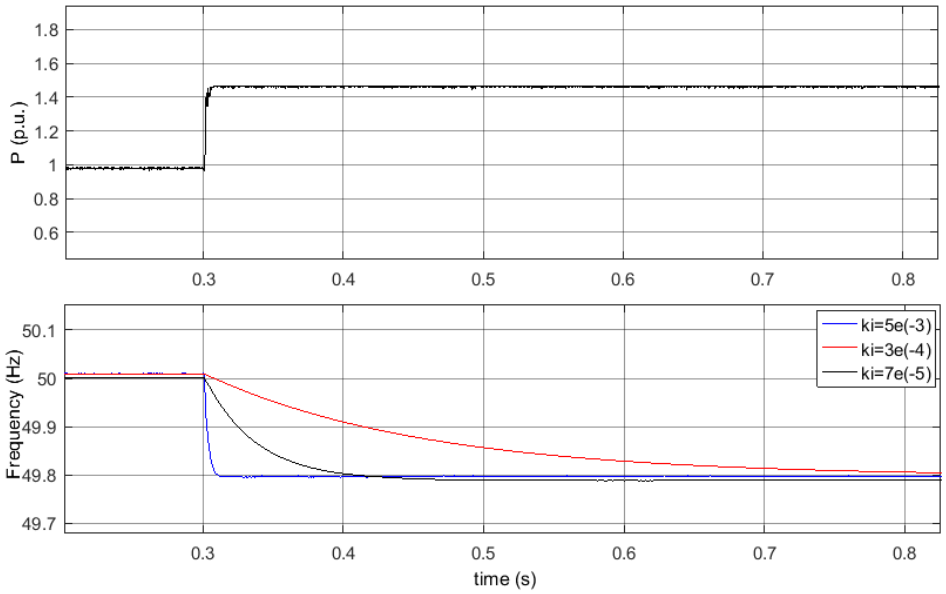

Figure 7.4: Scenario a.2: Frequency responses due to different k_i

Change in droop coefficient, K_f

According to Figure 4.6, K_f not only decides the final frequency value after the disturbance but also impacts its timely response. Figure 7.5 displays the results affected by different K_f (with $k_i = 3e^{-4}$). It indicates that the control scheme with swing equation provides a quite even response speed while the P-f rate is twice higher. This topology efficiently helps the system stability, because the value of K_f is various and regulated by demand management designs.

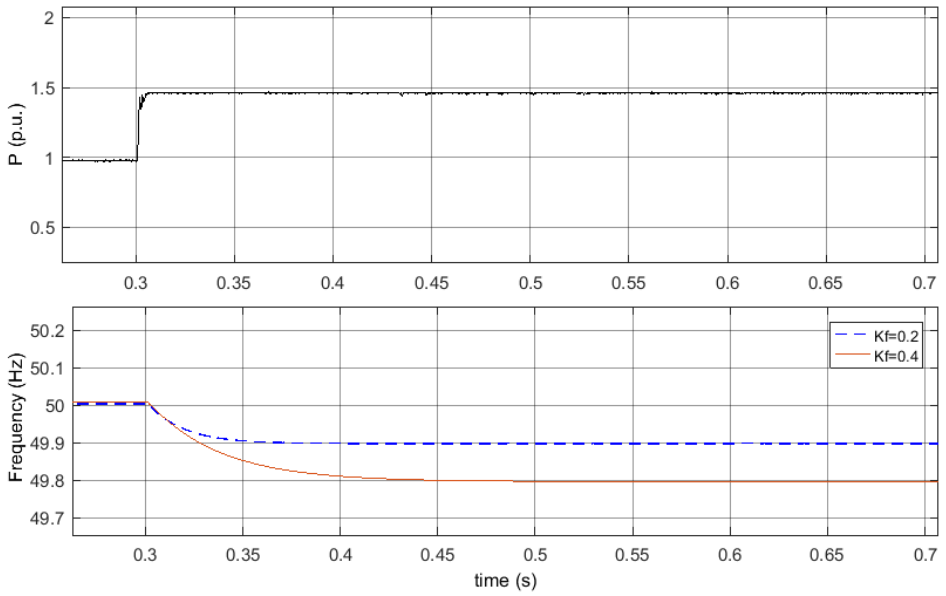

Figure 7.5: Scenario a.2: Frequency responses due to different droop coefficient, k_f

7.2.3. Scenario a.3: Setting a low-pass filter

The second method to improve the frequency behavior by combining a low-pass filter in the circuit.

Change in time coefficient, k

The low-pass filter imports a time delay into the investigated system. Figure 4.6 draws its core circuit, and Equation 4.9 expounds the principle. Coefficient k is used to adjust the extent of the delay. A higher value of k causes a larger time delay in the frequency response.

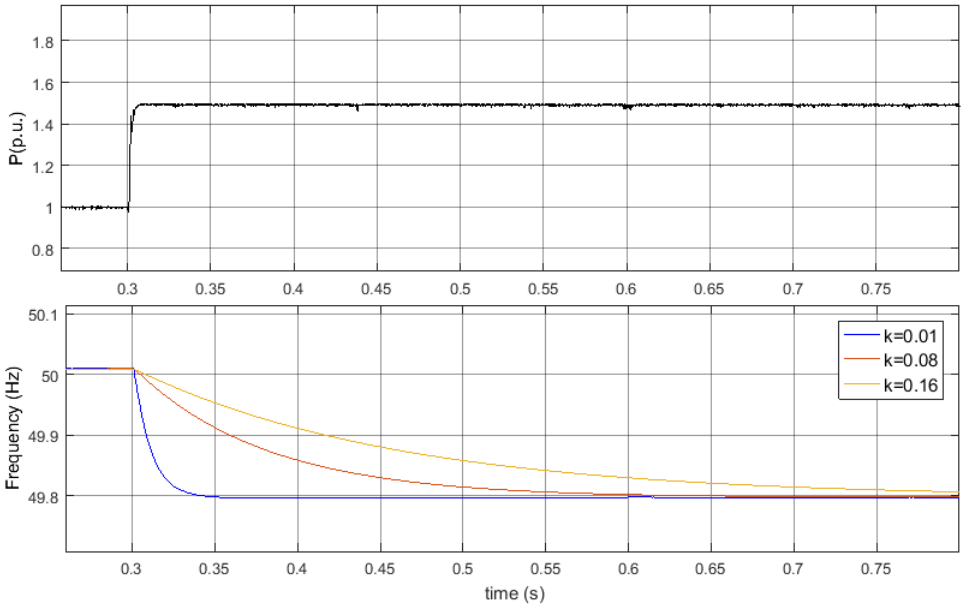

Figure 7.6: Scenario a.3: Frequency responses due to different time-delay coefficient, k

As the results shown in Figure 7.6, the low-pass filter leads a frequency performance, which is very close to the effects caused by the introducing the swing equation. Both of the integration part in the swing equation and the exponential item in the function of low-pass make the frequency time associated.

Change in droop coefficient, K_f

In the first approach, the real-time frequency dynamic behavior is also restricted by the factor K_f, acts as a parameter in the integration term. Seen in Equation 4.9, the reply via a low-pass filter does not have this characteristic, the output only concerns for the original response and involves a time delay. In this case, k keeps equal to 0.08. Figure 7.7 presents the result by different power-frequency curves, which shows that the rate of change of frequency doubles when the droop rate is increased by twice. It means that an equivalent incident can cause various output.

Considering the system reliability, the worst case should be identified. Besides the most

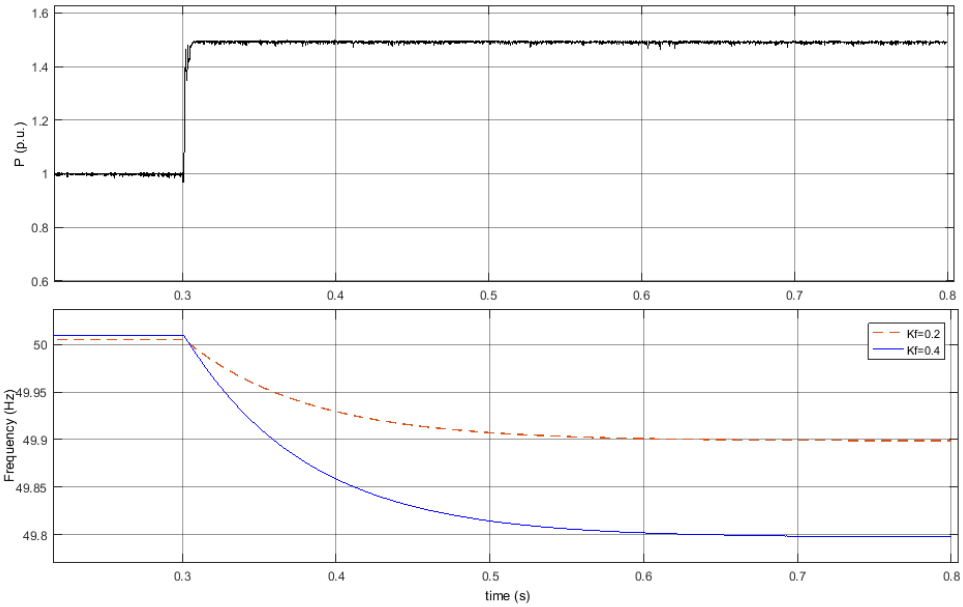

Figure 7.7: Scenario a.3: Frequency responses due to different droop coefficient, K_f

considerable disturbance, the largest $P - f$ rate should be taken into account when applying this approach.

7.2.4. Scenario a.4: Attaching a rate limiter

The rate limiter (RL), which restrains the rate of change of a signal, benefits the frequency behavior as well. Both of the critical rising and falling can be set in a RL. In this case, the two parameters are fixed mutually and distinguished by a positive and negative sign.

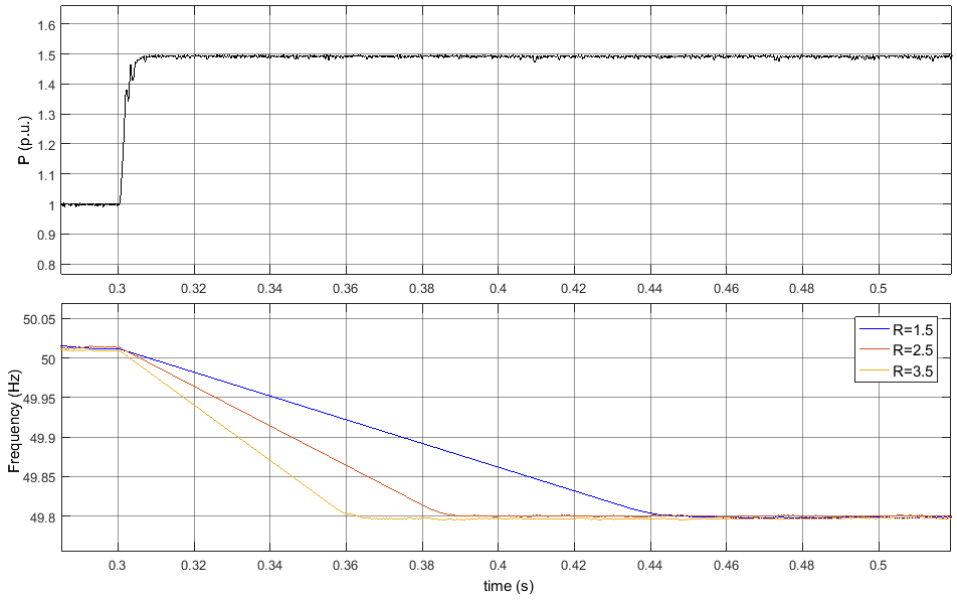

Figure 7.8: Scenario a.4: Frequency responses due to different boundary rates, $R(Hz/s$

Change in boundary rate, R

Figure 7.8 shows the dynamic responses of the voltage based MG to a change in the boundary of the RL in the system. As the rapidly original response shown in Figure 7.3, the output is restricted by the device during the whole state transformation.

Change in droop coefficient, K_f

The modify of the droop coefficient does not change the deviation rate of the output put. The performances due to different K_f are pretty alike, expect the variation time and the final state (Figure 7.8).

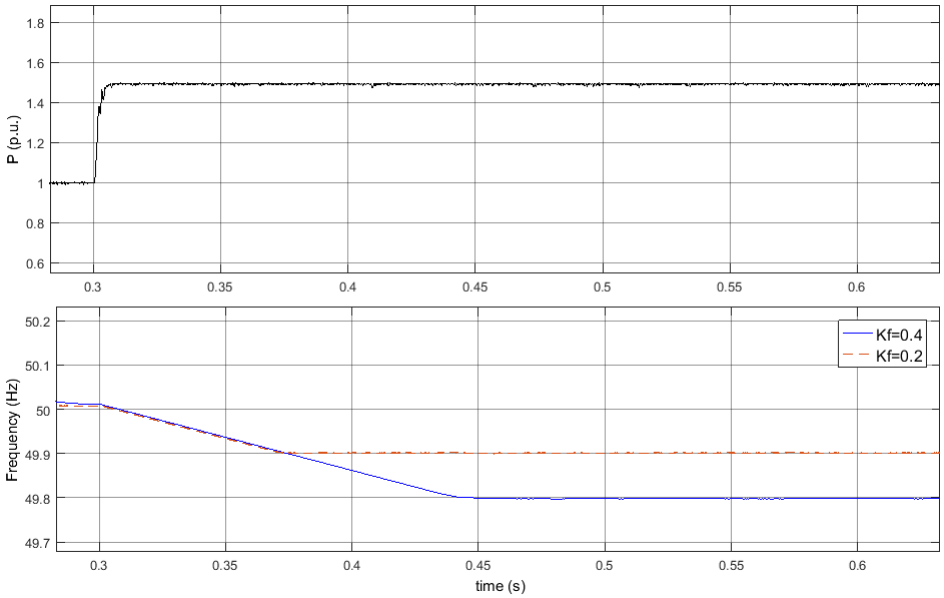

Figure 7.9: Scenario a.4-Frequency responses due to different droop coefficient, K_f

7.2.5. Discussion among three proposed approaches

The developed three methods are implemented and tested independently. All of the approaches efficiently improve the system frequency behavior. It is necessary to compare the advantage and disadvantage among the methods and try the effect combination by two methods.

The $Approach\ i$ emulate virtual inertia via transformation of the droop control loops and introduce the inertia property with an integration function. In this approach, the rate of change of frequency is considerably cut down, and the harmonics are removed. Moreover, the droop curve factor, K_f, is also made a factor of the frequency response function. In this way, the inertial stress keeps unchanged when K_f varies (verified in Figure /refa22). The drawback is that the parameters cannot be decided directly due to a particular RoCoF or a deviation period, because of the complexity of the algorithm.

$Approach\ ii$ holds relatively simpler control scheme and elements. But it has the same drawback with the first method for the exponential formula cannot be computed directly. Numerous tests and experiments are needed to find an appropriate time coefficient k. And the shift of droop factor K_f should also be taken into account.

Compare to the previous two methods; the rate limiter can regulate the changing rate directly by setting a limitation. And according to the adjusted rate boundary, the deviation period can be estimated, and it's directly correlated to the droop factor (seen in Figure 7.9).

In Figure 7.10, the system dynamic behaviors due to the original control loop and the three developed methods are presented. The deviation time zone is set the same by adjusting the related coefficients.

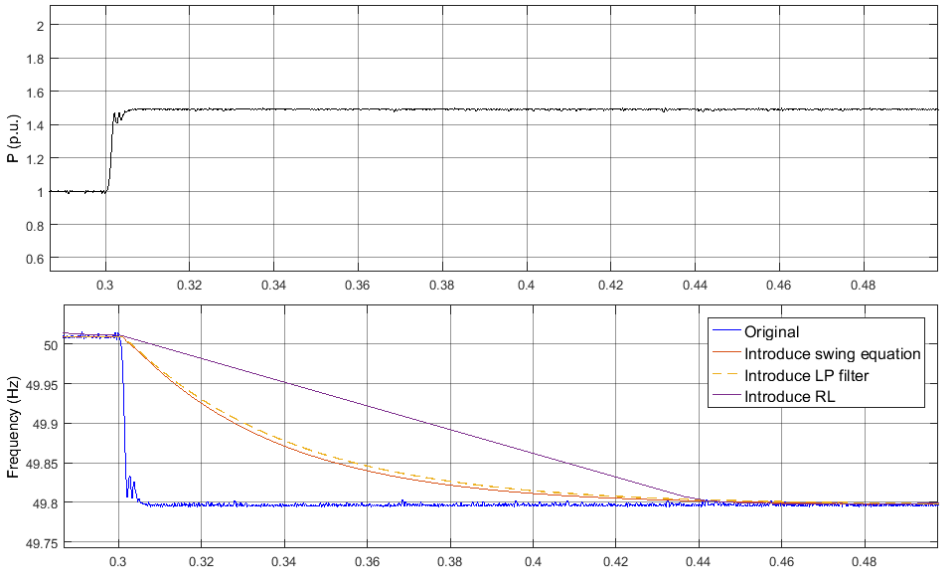

Figure 7.10: Scenario a.5: dynamic behaviors by the proposed methods within a fixed deviation period

From the results, the responses by the network with swing equation and with the low-pass filter are substantially alike, and the response difference is ignorable. In accordance with their equivalent performances in similar conditions, the method of introducing swing equation is more of advantage for it performs unrelated to the changing of droop curve.

Unlike the responses in the systems with the first two approaches, the RL results in a performance as straight line in this case. The selection of the topologies depends on the demand. If it's required to restrict the RoCof in the first milliseconds and preferred a smoother behavior, the combination of the $Apporach\ i$ and $Apporach\ iii$ could be the solution. Figure 7.11 shows the reaction of the mix of the two methods. It follows the rule of rate limiter in time zone before 0.37s and turns into the outcome with the swing equation control in the later period.

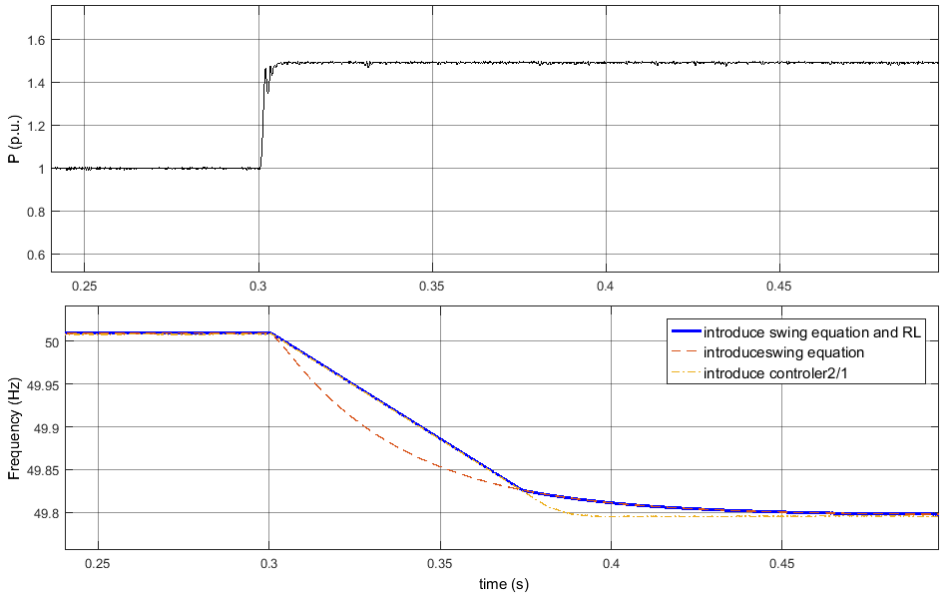

Figure 7.11: Scenario a.5: Combination of $Approach\ i$ and iii

7.3. Simulation results B: Islanded microgrid with diesel

7.3.1. Scenario b.1: current-source units based BESS with diesel

Based on the control blocker and algorithms in $Chapter\ 6$, the model of a current-source units based microgrid with a diesel engine is established in Matlab Simulink. In this scenario, a constant power reference is sent to the current source controller and diesel is used to supply to the rest of the power demand.

Figure 7.12 shows the network behaviors due to different levels of load change. From the presented results, the active power from the current source keeps around $0.5p.u.$ before and after the incident, which takes place at $t = 0.5s$. And the diesel covers the rest electric demand the disturbances during the state change. The terminal voltage decreases as the growth of the output because the load change influences the exciting current. A larger change leads to a more visible voltage drop. The node between the BESS and the grid shares the same voltage level with the diesel production since the inverter is set to track the grid voltage value and the effect of the transmission line is neglected. Considering the frequency response (the third row in the diagram), the RoCoF and overshoot are comparable higher with a greater disturbance. The frequency behaviors of the two source are precisely the same since one of the principles in the PQ controller is to follow the grid frequency. The supply of reactive power oscillates during the state transformation.

In this case, the most important signals are the active power and the frequency. The performances of voltage and reactive power are no longer presented in the later sections. And the most severe disturbance ($+0.5\ p.u.$) is selected for the following case study.

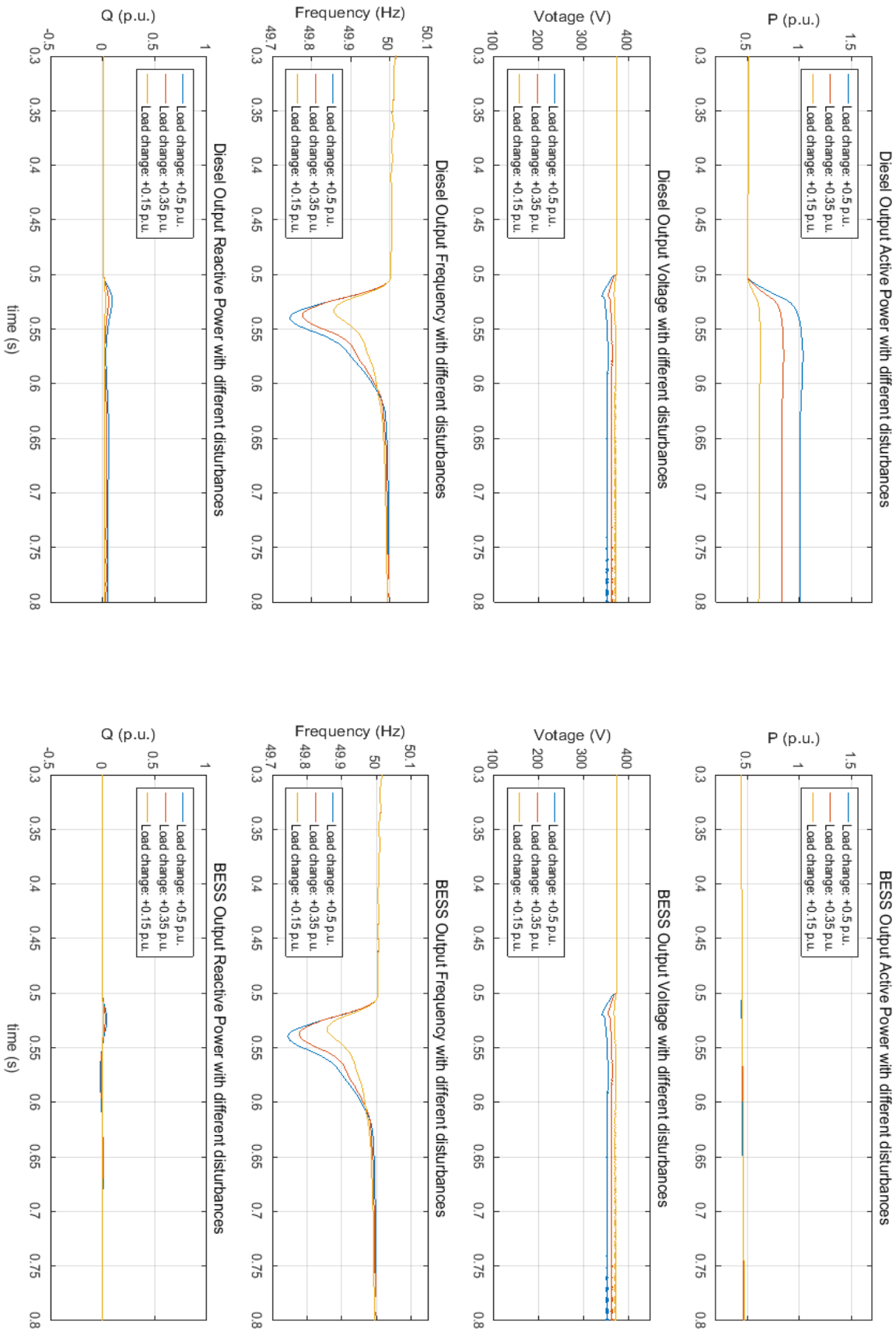

Figure 7.12: Scenario b.1: System responses due to different disturbances

7.3.2. Scenario b.2: Injecting inertia via a PID control

In Chapter 4, a PID control scheme for the BESS inverter is proposed to provide virtual inertia and damping force. The differential function (D control) introduces an additional the battery output, which transmits electricity energy as a function of frequency deviation rate. K_i is inertia coefficient, which arranges the inertia input by BESS.

Figure 7.14 shows the MG behaviors with different inertia factor K_i. The differential equation manages the BESS output. It presents as oscillation response (supply additional energy in the first 50 milliseconds and absorb positive power afterward). The increasing of the value of K_i leads to a higher overshoot and a quicker power change. Moreover, it smooths the power output from diesel and results in a slightly faster energy response for the whole grid. Regarding the frequency reactions, a larger K_i corresponds more significant time delay of the appearance time of valley, a slighter smaller overshoot and lower changing rate. It's noticeable that it leads a further system oscillation when K_i is set too high (the response when $K_i = 2000$).

According to the swing equation and Equation 4.14, an extra amount of inertia is injected into the system, e.p. when $K_i = 1000$, the system should obtain a $\Delta H = 500$ inertia quantity. It's obvious that the system doesn't have that much inertia property for the usual inertia amount for a synchronous machine is 3.5. The reason is that the current-source based BESS is not a current source which only use to provide inertia (introduced in Figure /refdiesel3). Figure 7.13 shows the comparison between the reference output of BESS and the measured value. There is a approximately 0.15 seconds time delay for the current source to response (for system reliability), which means the capability of improving for RoCoF is limited.

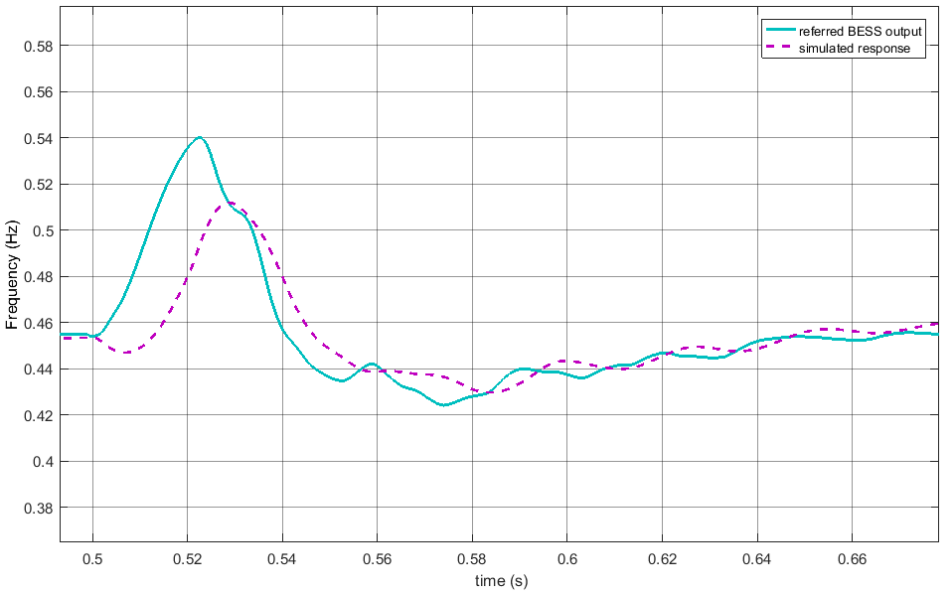

Figure 7.13: Scenario b.2: Reference BESS output and the measured value

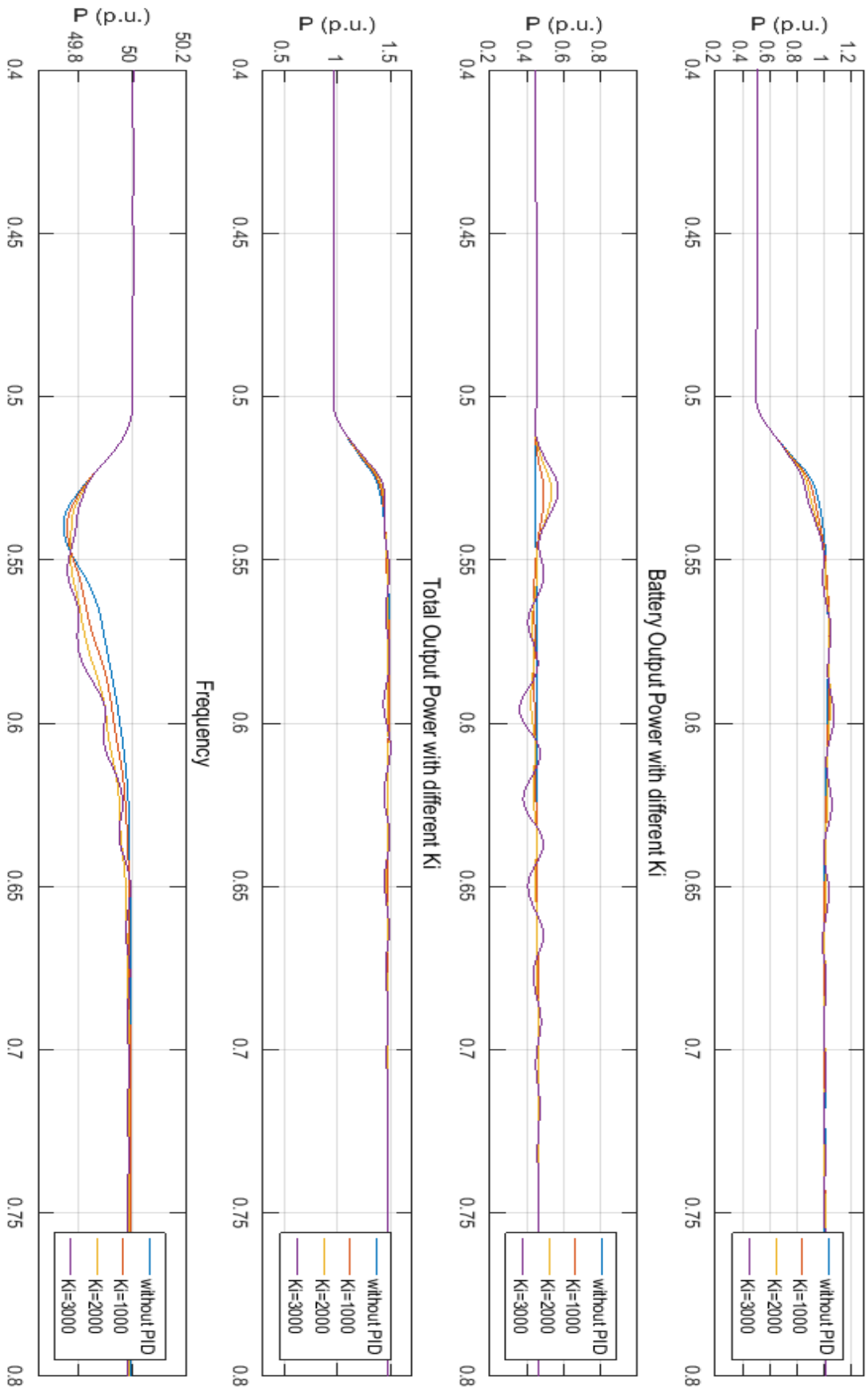

Figure 7.14: Scenario b.2: System responses due to different inertia coefficient, K_i

7.3.3. Scenario b.3: Injecting damping force via a PID control

The P (proportional) function in the PID controller produces the damping force. K_d is defined as the multiple of the frequency error. Figure 7.16 displays the system performance during the disturbance with different inertia factor K_i. BESS output is regulated by the proportional function. It provides extra power to compensate the power unbalance. The addition energy is directly proportional to the frequency error and the damping coefficient K_d. It smooths the power change in diesel, but the due to the whole system the power response become faster. A larger K_i bring forward the appearance valley, a relatively smaller overshoot in the frequency response. It's noticeable that it leads system unstable when K_d is set too high.

7.3.4. Scenario b.4: Frequency response with both additional inertia and damping property

By setting suitable values of coefficient K_i and K_d, both inertia and damping property can be emulated in the investigated islanded MG. The frequency behaviors are displayed in Figure 7.15. As seen in the result, the frequency response with both of the P and D control (dotted line) benefits from the addition control schemes. The overshoot is considerably cut off, the changing rate decreases dramatically after a period time-delay (explained in Figure 7.13), and the frequency goes back the nominal value in a smoother path.

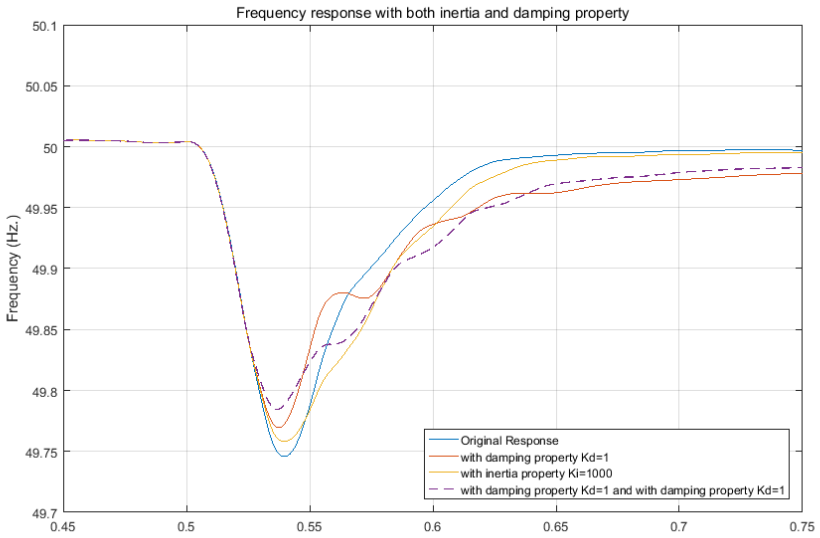

Figure 7.15: Scenario b.4: Frequency response with both additional inertia and damping property

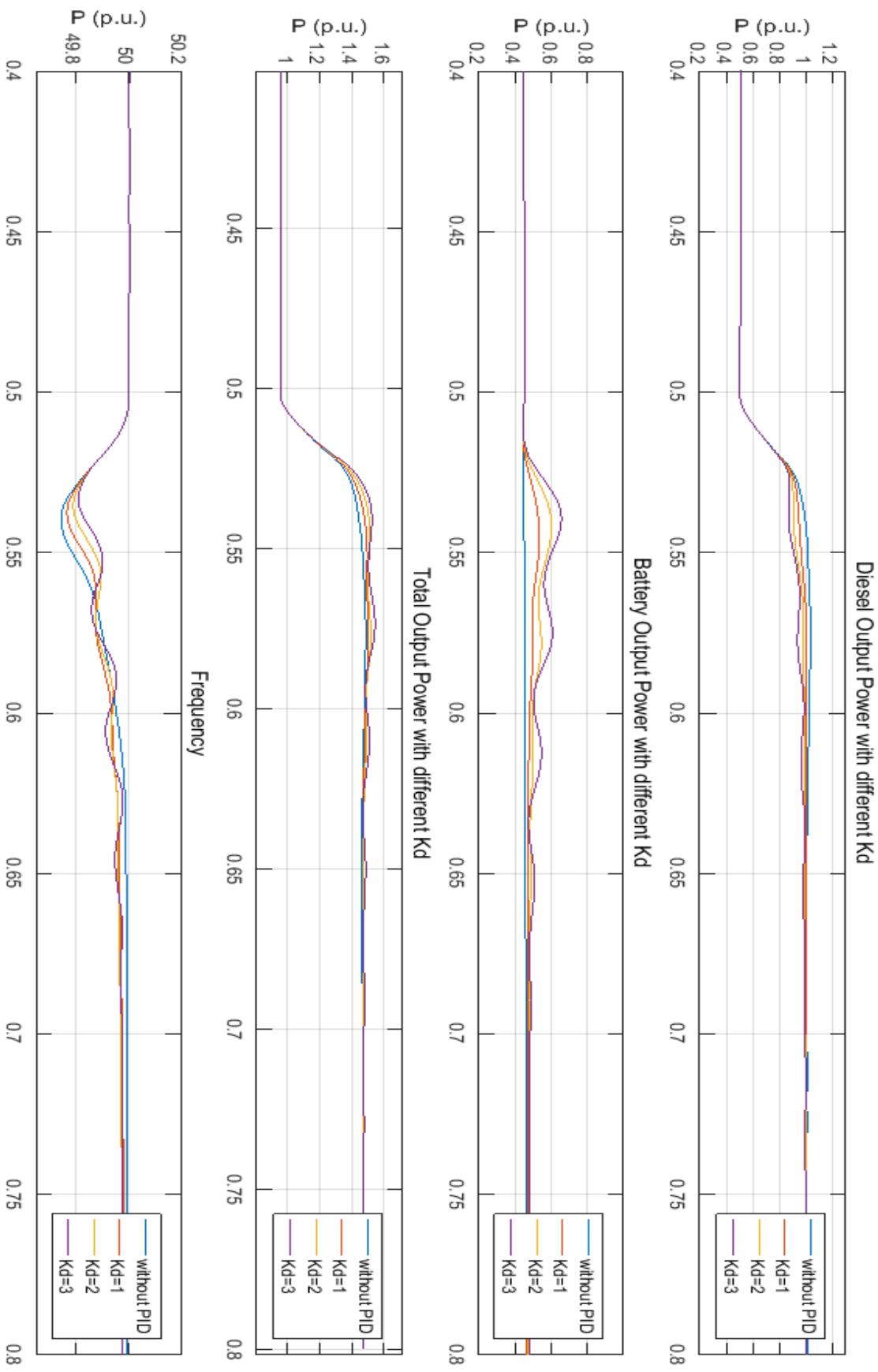

Figure 7.16: Scenario b.3: System responses due to different damping coefficient, K_d

7.4. Simulation results c: Comparison between voltage-source units based MG and current-source units based MGs with diesel

In Chapter 6, the mechanism schemes of the Voltage-Current control and Power-Current control are explained in detail. The different types of sources hold entirely different operating principles. For BESS working as a voltage source, methods are developed straightly to improve the frequency behavior. In terms of the current-source units based MG, extra PID controller manages BESS output to compensate the power imbalance in the grid, and it helps the frequency behavior. Comparisons are made in the two aspects, which could be the system active power output and grid frequency.

7.4.1. Scenario c.1: Comparison between the power response

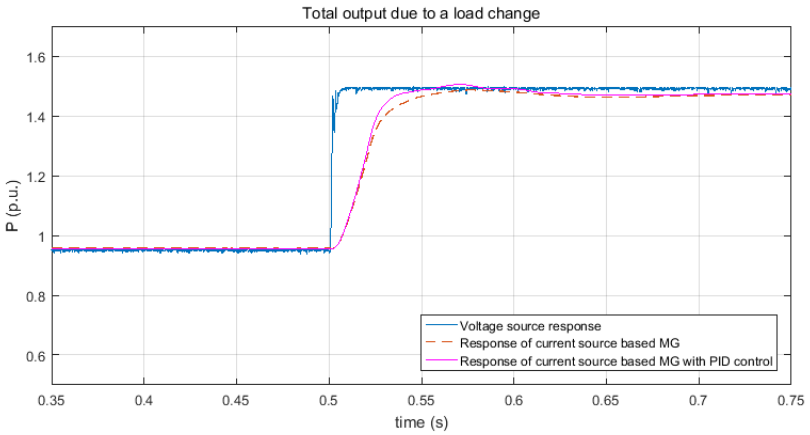

Figure 7.17: Scenario c.1: Total output of voltage source and current based MGs

Figure 7.17 shows the difference between the power responses of the voltage source and the current source-diesel multi-power supply. Seen from the simulation results, the power change of the voltage source acts as a 'step'. In not more than 10 milliseconds, its output increases from around 1 p.u to 1.5 p.u., and the new input load begins to operate immediately. On the contrary, the diesel has a much slower response, and it's takes 0.18 second for the diesel to cover the load raise. The participation of PID control on the BESS efficiently speeds up the state transformation (0.14 second for the total output growth).

7.4.2. Scenario c.2: Comparison between the frequency behavior

Figure 7.18 shows the responses of the two studied network with no additional control loops. The frequency deviation of the voltage source is set the same with the overshoot value in the current-source based MG by adjusting the coefficient K_f. The red curve presents a smooth droop of dynamic behavior because of the inherent inertia of a diesel engine. And it goes back

to the nominal state for the power-frequency characteristic in diesel.

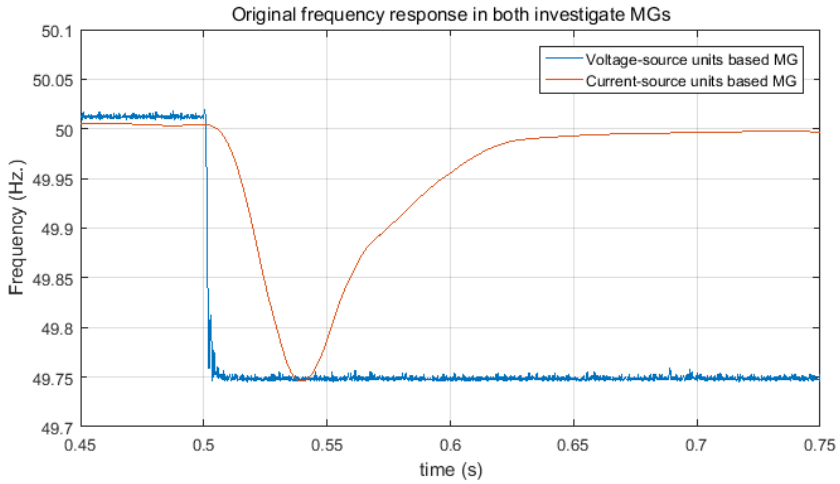

Figure 7.18: Scenario c.2: Original frequency responses of voltage source and current based MGs

The purposes of virtual inertia emulation in the two systems are entirely different. The objects of virtual inertia emulation in the two systems are completely different. The MG base on voltage units requires a gradual behavior in system frequency for demand side management. Regarding the MG composed by current-source units, the purpose turns to minimize the overshoot and cut down the rate of change of frequency. The idea response of the MG is a rapid power change (as the voltage source) with no frequency deviation. The developed frequency response is shown in Figure 7.19. The a frequency response via a rate limiter and swing equation represents the proposed 3 methods to improve frequency behavior in voltage source. The BESS working as voltage source fully controls the system frequency.

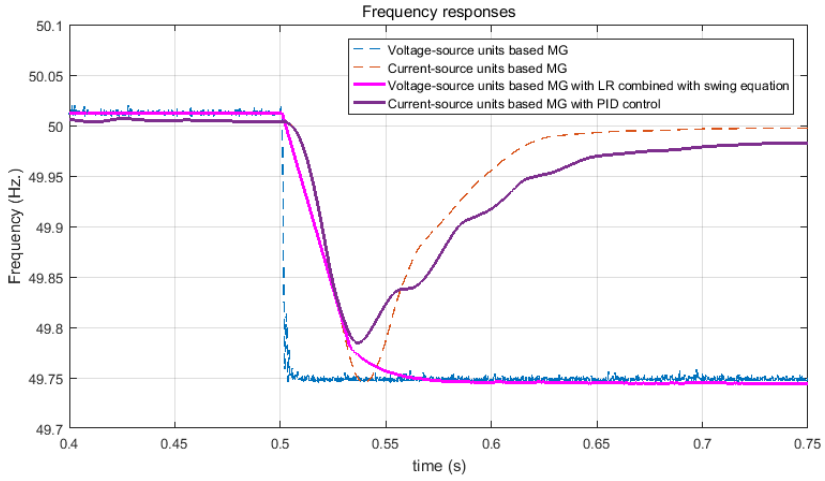

Figure 7.19: Scenario c.2: Frequency responses of voltage source and current based MGs

8

Conclusion and future work

8.1. Conclusions

Existing electronics methods for virtual inertia emulation in MGs have been found and compared. On top of previous approaches, in this thesis, novel approaches are developed and proposed to imitate inertial responses in both current-source and voltage-source based islanded MGs. Simulations and analysis of the investigated MGs in stand-alone mode are enabled by the corresponding dynamic models, which created in MATLAB Simulink graphical block diagramming tool.

In islanded MGs which use current sources as energy supply, advanced controllers are proposed to enhance the system stability.

- If the distributed RESs units (e.g. PV cells and wind turbines) straightly connect to the grid, additional control loops introduce frequency derivation formula into the controller of generation side converter. In cooperation with the MPPT, extra active power is transmitted or absorbed during frequency deviation. This method can be widely applied because of the large proportion of the converter based RESs units. The disadvantages are the energy waste to secure the provision of inertial power and the low-profit margin lead by added electronics components when many converters have participated.
- Since the significant mismatch between the unstable RESs and electricity demand exists, diesel is implicated to cut down the risk of blackouts. A short-term ESS is practiced to increase the inertia level. It stores energy as the kinetic energy in rotating mass and helps to stabilize the network when there is a state change. This approach does not cause energy dissipation, and it is convenient to be implemented in the completed systems. One of the difficulties of this method is to estimate the capacity of the ESS.

- Virtual Synchronous Generator control enables the battery energy storage system to mimic the dynamic behavior of a synchronous machine. This topology helps distributed RESs units replace the position of traditional generators, and it's available when the loads are predictable. Thus this method prefers the MGs in grid-connect mode or the isolated network with large size.

Voltage-source based islanded MGs are implemented when long-term storage systems are involved. By demand side management which includes load shedding and load shifting, it optimizes the size of batteries and improves the grid reliability. Frequency is recommended as the communication signal and interacts with a smart controller. It means particular groups of electrical devices operates at the specific frequency. Inertial frequency responses are expected to improve the efficiency and accuracy of supervision in loads. Three control schemes are developed and simulated.

- The dynamic behavior of BESS is able to imitate the rotor performance in swing equation by transforming the original droop control formula and adding a feedback control loop. The integral function cuts down the changing rate and removes the harmonics. Since droop control is a part of the proposed control circuit, the droop coefficient only decides the final state of a sudden change. To regulate the system behavior, the worse case (largest sudden change) should be considered, and the appropriate inertia coefficient should be set. With different values of inertia ratio, the RoCoF is restricted between tens and a few tenths of hertz per second while the response period varies from seconds to milliseconds. The integral part of the scheme increase the difficulty in predicting the system performance. If the behavior needs to be adequately controlled or predicted, tests due to all kinds of operation states transformations and different inertia coefficient should be done before the implementation of this method.

- A time delay in frequency response could be introduced by adding a low-pass filter with a comparatively large coefficient setting. The injected exponent function leads a continuous smooth frequency behavior, and the related factor controls postponing level. The maximum RoCoF can be estimated by the corresponded state space representation. The advantages of the approach are natural removing the harmonics and easy to be implemented. When there is a limitation for the highest deviation rate, the largest disturbance and the greatest droop value should be considered. The exponent function also influences the system supervision and prediction.

- The position to implicate the rate limiter is familiar to the low-pass filter. The signal from original droop control is regulated by the rate limiter and the final frequency value would not change. The most noticeable good point is that the particular frequency deviation ratio can be set, and will not be influenced by the adjustment of droop curve. Since the frequency response of original response is similar to step response, the output signal

may always follow the limitation value. In this way, the system frequency behavior is fully controlled and predictable.

- The combinations of the proposed methods are available. From the simulation results, the system regulated by both the swing equation and rate limiter has a nature response with precise ratio limitation. Since the controllers based on the swing equation and a rate limiter have the ability to minimize the impacts of the droop changing, one of the methods can be selected as the as the main controller. The suggestion is to use rate limiter cooperate with a low-pass filter which sets a comparably small factor to remove the harmonics.

The diesel-current source based isolated MG is simulated for the situation that energy from RESs is inadequate. In this case, additional inertia is to cut down the overshoot and decrease the RoCoF. According to the existing methods, a P(I)D is equipped to settle the reference active power signal. Besides a nominal preferred value (which is determined by the generation units state and the charge condition of battery), extra positive power is provided when system frequency shifts from its nominal value. The result of the differential equation of the frequency represents the injected inertia while the proportional term is regarded as a damping force. And the simulation results follow the characteristics of inertia and damping effect. It's not appropriate to compute the system inertia by summing up the inherent quantity and the injected value because the dead zone and a part of the sensitivity of the current-source BESS compromises on the system reliability. Overall, the implication of PID control speeds up the shift of energy transmission and minimizes the oscillation in frequency behavior.

Compared to the islanded MG electrified by current source based BESS and diesel, the performance of energy states transformations in the voltage-source units based MGs is ideal, and the inverter dominates the system frequency. Inertial control schemes serve for the demand side management and optimize the operation performance. On the other hand, the addition inertia property in current source based MGs is used to support the energy supply and reduce the impacts of disturbances.

8.2. Further work

For voltage source based MGs, testing the proposed methods in a muti-cell based system, in which the isolated MGs are connected to a backbone, would contribute to the work of extending the MGs size and the enhancing its stability. In this condition, the output of MG cells should be ruled, which could be a master-slave mode (the cells follows the behavior of a master) or an automatic scheme (all the cells keep following their droop curves). The appropriate method to emulate virtual inertia should be selected.

The approach to emulate virtual in current-source based MGs would be much more strong if a self-turning coefficient is implicated. To realize this approach, a "RoCoF" estimation process is

required,where the value of K_i in the implicated PID controller could be adjusted according to the estimated rate changing ratio, could be included. In other words, a ratio detector which is used to compute the derivative rate (similar to the calculation progress in the rate limiter).

- When the estimated RoCoF is with in the allowable range, the PID controller operates with the original setting value of K_i and K_d.
- When the estimated RoCoF exceeds the range, then the D controller is adjusted. The amount of injected inertia (K_i) is increased until the RoCoF would lie within the proper range.

Bibliography

[1] P. Kundur, N. J. Balu, and M. G. Lauby, *Power system stability and control*, Vol. 7 (McGraw-hill New York, 1994).

[2] J. Machowski, J. Bialek, and J. Bumby, *Power system dynamics: stability and control* (John Wiley & Sons, 2011).

[3] P. Kundur, J. Paserba, V. Ajjarapu, G. Andersson, A. Bose, C. Canizares, N. Hatziargyriou, D. Hill, A. Stankovic, C. Taylor, *et al.*, *Definition and classification of power system stability ieee/cigre joint task force on stability terms and definitions,* Power Systems, IEEE Transactions on **19**, 1387 (2004).

[4] D. W. Gao, *Energy Storage for Sustainable Microgrid* (Academic Press, 2015).

[5] T. Vral, *Frequency Based μGrid Control*, Internship Report (Alfen bv, 2015).

[6] A. V. Souto, *Optimization and energy management of a microgrid based on frequency communications*, MSC thesis (Tudelft, 2016).

[7] G. Lalor, J. Ritchie, S. Rourke, D. Flynn, and M. J. O'Malley, *Dynamic frequency control with increasing wind generation,* in *Power Engineering Society General Meeting, 2004. IEEE* (IEEE, 2004) pp. 1715–1720.

[8] J. Ekanayake and N. Jenkins, *Comparison of the response of doubly fed and fixed-speed induction generator wind turbines to changes in network frequency,* Energy conversion, IEEE transactions on **19**, 800 (2004).

[9] S. I. Nanou, A. G. Papakonstantinou, and S. A. Papathanassiou, *A generic model of two-stage grid-connected pv systems with primary frequency response and inertia emulation,* Electric Power Systems Research **127**, 186 (2015).

[10] Y. Chen, R. Hesse, D. Turschner, and H.-P. Beck, *Improving the grid power quality using virtual synchronous machines,* in *Power engineering, energy and electrical drives (POWERENG), 2011 international conference on* (IEEE, 2011) pp. 1–6.

[11] M. Van Wesenbeeck, S. De Haan, P. Varela, and K. Visscher, *Grid tied converter with virtual kinetic storage,* in *PowerTech, 2009 IEEE Bucharest* (IEEE, 2009) pp. 1–7.

[12] Y. Hirase, K. Abe, K. Sugimoto, and Y. Shindo, *A grid connected inverter with virtual synchronous generator model of algebraic type,* IEEJ Transactions on Power and Energy **132**, 371 (2012).

[13] M. Torres and L. A. Lopes, *Virtual synchronous generator control in autonomous wind-diesel power systems,* in *Electrical Power & Energy Conference (EPEC), 2009 IEEE* (IEEE, 2009) pp. 1–6.

[14] L. Zeni, A. J. Rudolph, J. Münster-Swendsen, I. Margaris, A. D. Hansen, and P. Sørensen, *Virtual inertia for variable speed wind turbines,* Wind Energy **16**, 1225 (2013).

[15] A. J. Wood and B. F. Wollenberg, *Power generation, operation, and control* (John Wiley & Sons, 2012).

[16] S. R. Roy, O. Malik, and G. Hope, *An adaptive control scheme for speed control of diesel driven power-plants,* Energy Conversion, IEEE Transactions on **6**, 605 (1991).

[17] S. Roy, O. Malik, and G. Hope, *A low order computer model for adaptive speed control of diesel driven power-plants,* in *Industry Applications Society Annual Meeting, 1991., Conference Record of the 1991 IEEE* (IEEE, 1991) pp. 1636–1642.

[18] S. Roy, O. Malik, and G. Hope, *A least-squares based model-fitting identification technique for diesel prime-movers with unknown dead-time,* Energy Conversion, IEEE Transactions on **6**, 251 (1991).

[19] H. Bevrani, T. Ise, and Y. Miura, *Virtual synchronous generators: a survey and new perspectives,* International Journal of Electrical Power & Energy Systems **54**, 244 (2014).

[20] K. Sakimoto, Y. Miura, and T. Ise, *Stabilization of a power system with a distributed generator by a virtual synchronous generator function,* in *Power Electronics and ECCE Asia (ICPE & ECCE), 2011 IEEE 8th International Conference on* (IEEE, 2011) pp. 1498–1505.

[21] S. D'Arco, J. A. Suul, and O. B. Fosso, *A virtual synchronous machine implementation for distributed control of power converters in smartgrids,* Electric Power Systems Research **122**, 180 (2015).

[22] W. Yang, *Research on Microgrids operation and control schemes*, MSC thesis (Southwest Jiaotong University, 2015).